Habilitationsschrift
zur
Erlangung der Venia legendi
für das Fach Physik
der
Ruprecht–Karls–Universität
Heidelberg

vorgelegt von
Teresa Marrodán Undagoitia
aus Eibar (Spanien)

2014

Revealing the nature of dark matter with XENON

Habilitation summary
by
Teresa Marrodán Undagoitia

March 2014

Contents

Chapter 1

Introduction

The existence of a new form of non-luminous matter is indicated by a variety of cosmological and astronomical observations. It is commonly assumed that elementary particles could be the constituents of this 'dark' matter. New particles that could account for dark matter appear in various theories beyond the standard model of particle physics and could be detected via their scattering in a detector medium. A measurement of this process would provide information on the dark-matter particle mass and its interaction probability with ordinary matter. This chapter summarises the current indications for dark matter, presents possible candidates and ways of detecting them, focussing on particle dark-matter candidates. Finally, the direct detection principles and the status of the experimental results are reviewed.

1.1 Indications for dark matter from Astronomy and Cosmology

Indications for non-luminous matter appear in our Universe at very different scales. Jan H. Oort mentioned dark matter already in 1932 to explain the dynamics of stars in our Galaxy [1]. Observations of the dispersion velocities of nebulae in the Coma cluster brought also Fritz Zwicky [2] to the idea that a large amount of dark matter could be responsible for the high velocity values measured. In 1978, Vera C. Rubin *et al.* [3] found that rotation velocities of stars in galaxies stay approximately constant with increasing distance to their galactic center. This observation was in contradiction with the expectation as objects outside the visible mass distribution should have velocities $v \propto 1/\sqrt{r}$ following Newtonian dynamics. A uniformly-distributed halo of dark matter could explain both the dispersion velocities in clusters and the rotation velocities of objects far from the luminous matter in galaxies. Historically, these are the first indications for dark matter.

A further hint for the existence of dark matter arises from gravitational lensing measurements [4]. This effect discussed by Albert Einstein [5] in 1936 and later by Zwicky [6] occurs when a massive object is in the line of sight between the observer at the Earth and the object under study (observable). The light-rays are deflected through their path due

to the gravitational field resulting in, e.g., multiple images or a deformation of the image of the observable (strong and weak lensing, respectively). The degree of deformation can be used to reconstruct the gravitational potential of the object that deflected the light along the line of sight. From various observations it has been found that the reconstructed mass using this method is greater than the luminous matter, resulting in very large mass to light ratios (from a few to hundreds). Gravitational lensing has also been applied in rare galaxy-cluster collisions to reconstruct the mass distributions in such events where mass to light ratios of > 200 are measured. In some examples [7][8][9], the mass distributions appear clearly separated from the main constituent of the ordinary matter, i.e. the gas clouds which collide and produce detectable X-rays. This can be interpreted as being due to dark matter haloes that continue their trajectories relatively independent of the collision. A weak self-interaction cross-section for dark matter can be derived from these observations. Further examples show a displacement of the matter distribution from the collision of the gas clouds [10][11] but the extraction of dark matter self-interaction properties becomes challenging/controversial due to different reconstructed mass profiles [12][13].

Precise measurements of the cosmic microwave background (CMB) anisotropies by WMAP [14] and more recently by the Planck satellite [15] show the Universe when it was about 400 000 years old. The power spectrum of density fluctuations can be evaluated by a six parameter model which gives access to the baryonic matter, dark matter and dark energy contents of the Universe. This cosmological standard model, which fits the data with high significance, is denoted ΛCDM (Λ cold dark matter) indicating that dark matter with a small random velocity is a fundamental ingredient. The Λ refers to the cosmological constant necessary to explain the current accelerating Universe [16]. Baryon acoustic oscillations, i.e. periodic fluctuations in the density of the visible matter caused by acoustic waves which existed in the early Universe at the time before decoupling of photons from matter, produce characteristic ripples in the CMB spectrum. From the relative height of these ripples, the amount of dark matter relative to the total energy in the Universe can be determined. Present estimates [17] show a flat Universe with $\Omega_{\mathrm{DM}} = 0.27$, $\Omega_b = 0.049$ and $\Omega_\Lambda = 0.69$ representing the densities of dark matter, baryonic matter and dark energy, respectively.

In the standard scenario, quantum fluctuations during inflation result in the anisotropies of the CMB. To propagate matter distributions from the time when recombination happened to the present state, N-body simulations of dark matter particles have been carried out [18]. For instance, the Millennium simulation [19] propagates 10^{10} particles using super computers in order to describe the growth of cosmic structure from large size down to $\sim 10\,\mathrm{kpc}$ objects. Meanwhile this type of simulations reproduce very accurately the measurements made by galaxy surveys [20]. Measurements of the Lyman$-\alpha$ forest [21] and weak lensing [22] confirm the cosmic structure considering not only galaxies but also gas clouds and non-luminous matter. These dark matter-only simulations have been used to determine the structure formation which serves as seed for galaxy and cluster formation. Recently, gas and stars have been included into the simulations and it is shown that they can significantly alter the distribution of the dark matter component [23].

1.2 The nature of dark matter: possible candidates

Massive astrophysical compact halo objects (MACHOs) have been considered as a possible explanation for the large mass to light ratios detected in astronomy. These objects could be black holes, neutron stars, brown dwarfs or unassociated planets and would emit very little to no radiation. Searches for such objects using gravitational microlensing [24] showed that they can make up about 20% of the dark matter in our galaxy and that a halo made 100% out of MACHOs is ruled out at 95% confidence level [25]. Another plausible solution to describe some of the astronomical measurements mentioned in section 1.1 is to modify gravitation to accommodate the observations. Such modified newtonian dynamic models like MOND [26] or its relativistic extension TeVeS [27] can, for example, successfully describe rotational velocities measured in galaxies. On larger scales however, MOND fails or needs unrealistic parameters to fit observations of these striking phenomena.

A more common ansatz is to assume that dark matter is made out of massive neutral particles featuring a weak self-interaction. From the known particles in the standard model, only the neutrino can be considered. Due to its relativistic velocity in the early universe, the neutrino would constitute a hot dark matter candidate. Cosmological simulations have shown, however, that a Universe dominated by neutrinos would not be in agreement with the observed clustering scale of galaxies [28]. Also, due to phase-space density arguments, neutrinos cannot be tightly packed into galaxy halos [29]. Sterile neutrinos are hypothetical particles which were originally introduced to explain the smallness of the neutrino masses. In addition, they could play an important role in astrophysics, in particular, sterile neutrinos could account for warm/cold dark matter depending on the production mechanism [30]. The masses which are not yet constrained by X-ray measurements or the analysis of dwarf spheroidal galaxies range from 1 keV to tens of keV. Given this very low mass and the low interaction strength, its existence cannot be accessed by direct detection experiments. An indication could, however, arise from the X-ray measurement of the sterile neutrino decay via the radiative channel $N \rightarrow \nu\gamma$ [31].

Models beyond the standard model of particle physics suggest the existence of new particles which could account for the dark matter. If such particles would be stable, neutral and have a mass from below GeV/c^2 to several TeV/c^2 they could thus be the weakly interacting massive particle (WIMP). The standard production mechanism for WIMPs assumes that in the early Universe these particles were in equilibrium with the thermal plasma [32]. As the Universe expanded, the temperature of the plasma became lower than the WIMP mass resulting in the decoupling from the plasma. At this freeze-out temperature, when the WIMP annihilation rate was smaller than the Hubble expansion rate, the WIMP production rate is such that the dark matter relic density is reached. The cross section necessary to observe the current dark matter density is of the order of the weak interaction scale. It appears as a great coincidence that a particle interacting via the weak force would produce the right relic abundance and therefore the WIMP is a theoretically well motivated dark matter candidate. The neutralino is the lightest particle in some Supersymmetry models [33] and constitutes an example of a new particle fulfilling the WIMP properties. WIMP searches carried out by the XENON100 experiment are

presented in chapter 3.

In the standard model of particle physics, there is no fundamental reason why QCD should conserve P and CP. However, from the experimental bound on the neutron electric dipole moment [34], very small values of P and CP violation result. In 1977, a new symmetry was postulated by Roberto Peccei and Helen Quinn [35] in order to solve this so-called 'strong CP-problem' [36]. When this symmetry is spontaneously broken, a new particle called axion appears. The axion mass and the coupling strength to ordinary matter are inversely proportional to the breaking scale which was originally associated to the electroweak scale. This original axion model was experimentally ruled out by laboratory experiments [37]. Cosmological and astrophysical results provide as well very strong bounds on the axion hypothesis [36]. There exist, however, further 'invisible' axion models in which the breaking scale is a free parameter, KSVZ [38][39] and DFSZ [40][41], but still provide a solution to the CP-problem. Invisible axions would have been produced non-thermally in the early Universe by mechanisms like the vacuum realignment [42][43] for example, giving the right dark matter abundance. The resulting velocity dispersion would be small and therefore these axions are a cold candidate. For certain parameters, axions could account for the complete missing matter [44]. Chapter 4 discusses possible searches for axions using liquid xenon detectors and specifically in XENON100.

Sterile neutrinos, supersymmetric particles and axions are by far not the only particle candidates for dark matter. Other candidates like the Kaluza-Klein particle in models with extra-dimmensions (see recent update [45]), little Higgs, SuperWIMPs (super-weakly interacting massive particle produced as a decay of WIMPs) could also be the answer to the dark matter nature. Further information can be found in [46].

1.3 Searches for dark matter particles

If particles are the answer to the dark matter puzzle, there are three main possibilities to verify this: to produce them at particle accelerators, to look for products of their self-annihilations at locations where dark matter clusters or to directly detect these particles via scattering off a detector's target material.

Since the start of the large hadron collider (LHC) at CERN in 2008, the CMS [47] and Atlas [48] experiments have searched for new particles in proton collisions at a center-of-mass energy of 7 TeV. Besides the discovery of the Higgs particle [49][50], CMS and Atlas have studied a number of new particle signatures by scanning the parameter space of different supersymmetric and extra-dimensions models. The presence of a new particle would only be inferred by observing events with missing transfer momentum. Therefore, events with, e.g., an energetic jet and an imbalance momentum transfer are selected for analysis. The results so far are consistent with the standard model expectations [51][52] but further searches will be performed in the next years. The derived bounds can be translated into limits on the cross section for a given particle mass. These bounds are most constraining below 5 GeV and 200 GeV for spin-dependent and spin-independent interactions, respectively.

Dark matter particles can gravitationally accumulate in astrophysical objects such as stars, galaxies or our Sun. Consequently, the enhanced self-annihilation or decay into standard model particles could produce a measurable flux. The detection of this secondary particles is a further detection mechanism usually denoted as 'indirect detection'. Large neutrino detectors like Ice Cube are able to search for dark matter annihilations into neutrinos. No evidence for such a signal has been observed yet and limits on the cross section are derived [53] (see also figure 3.4). Cherenkov telescopes for TeV γ-ray detection can look specifically in the direction of objects where a large amount of dark matter is expected. Either a γ-flux in dwarf galaxies or galaxy clusters, or mono energetic line signatures are searched for. So far no significant signal from dark matter annihilations has been measured and upper limits are derived by the MAGIC [54], HESS [55] and VERITAS [56] telescopes. Indirect searches can be also performed by satellites capable of detecting low-energy γ-rays like Fermi [57]. The detection of a line-like feature at 130 GeV has been reported in the literature but a posterior analysis performed by the Fermi collaboration finds only weak significance for this signal in one of the five regions studied. In addition, the width of the feature is narrower than the expected energy resolution of the device at the level of $(2-3)\,\sigma$ [58]. Finally, also charged particles like protons, antiprotons, electrons and positrons can be detected by satellites. Measurements on the steadily increasing positron fraction from 10 to ~ 250 GeV by Pamela [59] and AMS [60] rise discussions on its possible dark matter origin. However, given that such a spectrum could be also described by astrophysical objects as pulsars (rapidly rotating neutron stars), this cannot be considered as a clear dark matter signal indication.

The third detection mechanism, the direct detection of a target recoil caused by a dark matter particle interaction, is the topic of this work and will be described in more detail in the following. Section 1.4 describes the main ingredients of this method and section 1.5 reviews the current status of direct searches.

1.4 Principles of direct detection

During the last years, large efforts have been pursued to develop experiments which are able to directly test the hypothesis that dark matter consists of new particles. The signature of dark matter in a direct detection experiment would consist of a recoil spectrum of single scatter events. In case of a WIMP, a nuclear recoil is expected [61]. Detectors with the capability to distinguish between nuclear and electronic recoils have been developed, as the main background for a WIMP search is due to electronic recoils from natural γ and β-decaying isotopes. Another possible dark matter signature is the so-called 'annual modulation'. As a consequence of the Earth rotation around the Sun, the flux of dark matter particles from the Milky Way halo should be larger around June and smaller around December. This effect was pointed out in the middle of the 80s [62]. The rate modulation would enhance the ability to discriminate against background and help to confirm a detection. In addition to the rate, the direction of the incoming particles would be on average opposite to each other in June and December [63].

In order to identify non ambiguously interactions from dark matter particles, ultra-low background conditions are required. Therefore, dark matter detectors are typically located in underground laboratories where the cosmic radiation and its reaction products are strongly reduced. Furthermore, the detector medium and materials in the vicinity of the target need to have low concentrations of radioactive decaying isotopes. Long term stability is as well required as several years of data are typically acquired. In addition, large detector masses of hundreds of kg to few tons are necessary to acquire significant statistics of the rare dark matter interactions.

In general, the differential recoil spectrum resulting from dark matter interactions is expected to be featureless and decreasing with energy. It can be written following [64] as

$$\frac{dR}{dE}(E,t) = \frac{\sigma \cdot \rho_0}{2\mu_\chi^2 \cdot m_\chi} \cdot F^2(E) \cdot \int \frac{f(v,t)}{v}\, \mathrm{d}^3 v, \tag{1.1}$$

σ and m_χ are the WIMP cross section with nuclei and its mass, respectively and are the parameters of interest for a dark matter experiment. μ_χ^2 is the WIMP-nucleon reduced mass and $F^2(E)$ is the form factor correction (factor <1) due to the finite size of the target nucleus. Equation 1.1 shows also the astrophysical parameters explicitly, ρ_0 is the dark matter density and $f(v,t)$ accounts for the WIMP velocity distribution in the Earth reference frame. The velocity distribution is time dependent due to the movement of the Earth around the Sun.

The mass, extent and shape of the dark matter halo are still uncertain parameters in astronomy. A local dark matter density of $0.3\,\mathrm{GeV/cm^3}$ results from mass modelling of the Milky Way using parameters in agreement with observational data [65]. However depending on the profile model used for the halo, a density range from $(0.2-0.4)\,\mathrm{GeV/cm^3}$ can be derived. For the dark matter velocity profile, commonly a truncated Maxwell-Boltzmann distribution with a local circular speed of 220 km/s is used. This standard value for the circular velocity results from an average of values found in different analyses [66]. More recent analyses using additional data find velocities from $(200 \pm 20)\,\mathrm{km/s}$ to $(279 \pm 33)\,\mathrm{km/s}$ [65]. The escape velocity defines a cut-off in the description of the halo profile. The standard value of 544 km/s is the likelihood median calculated using data from the RAVE survey [67], the 90% confidence interval contains velocities from 498 km/s to 608 km/s. The large ranges of possible values for the dark matter density, circular and the escape velocity illustrate that the uncertainties in the halo modelling are significant. Besides the uncertainties on these parameters, numerical simulations provide different halo profiles, see [68][69][70][71]. The GAIA satellite [1] is in orbit since January 2014 and plans to measure about a billion stars in our Galaxy and throughout the Local Group. These unprecedented positional and radial velocity measurements will reduce the uncertainties on the local halo model. Using the standard values, nuclear recoils of $(1-100)\,\mathrm{keV}$ are expected for WIMPs with masses of $(10-1000)\,\mathrm{GeV}/c^2$.

For WIMP interactions that are independent of spin, it is assumed that neutrons and protons contribute equally to the scattering process (isospin conservation). For sufficiently low momentum transfer, q, the amplitudes add in phase and give a coherent cross

[1] http://sci.esa.int/gaia

section which is proportional to A^2. For spin-dependent interactions, only unpaired nucleons contribute to the scattering. Therefore, only nuclei with an odd number of protons or neutrons are sensitive to these interactions. In this case, the cross section is related to the quark spin content of the nucleon with components from both proton and neutron couplings. When the momentum transfer is such that the particle wavelength is no longer large compared to the nuclear radius, the cross section decreases with increasing q. As shown above, the form factor F accounts for this effect and the cross section can be expressed as: $\sigma \propto \sigma_0 \cdot F^2$, where σ_0 is the cross section at zero momentum transfer. For spin independent interactions of WIMPs, the form factor is calculated assuming a distribution of scattering centres to be the same as the charge distribution derived from electron scattering experiments [64] and the Helm parametrisation [72] is commonly used. For spin-dependent interactions, the form factor is written in terms of the spin structure function whose terms are determined from nuclear model calculations [73][74][75]. A common practice is to express the cross section for the interaction with protons, σ_p, and with neutrons, σ_n (see section 3.4).

The result of a dark matter experiment is an event rate with a certain spectral shape. If this rate is significantly higher than the expected background, a signal can be claimed. Typically a standard halo model is assumed, in order to express the results in the cross section versus dark-matter-mass parameter space. A signal would be represented by probability contours in this representation. If the rate observed is compatible with the background expectation, exclusion limits are derived. Those have a characteristic V-shape [64], the rise at low masses is due to the detector threshold, while at high masses it is a consequence of a fixed dark matter density. It has been noted that the choice of a different halo model affects the comparability of results from experiments using different target materials. Therefore, an alternative representation of the data which integrates out astrophysical uncertainties has been recently proposed [76].

1.5 Current experimental results and possible interpretations

Among all current direct dark matter experiments, few have measured an excess of events or show distinctive signatures that can be interpreted as being due to dark matter particles. Most important is the measurement by the DAMA experiment which records the scintillation rate of low-radioactive NaI(Tl) crystals. The data of DAMA and its successor DAMA/LIBRA showed an annual-modulated single-hit rate, the maximum of which is compatible with June 2 nd within $2\,\sigma$. This is the expected phase for dark matter interactions. Meanwhile, the significance of this signal is at $8.9\,\sigma$ over a measurement of 13 annual cycles [77]. A similar modulation signal has been recently shown in the CoGeNT experiment [78], however, the modulation hypothesis is preferred over the null hypothesis only at $2.2\,\sigma$. This detector consists of p-type point-contact germanium detectors with a very low energy threshold of 0.5 keV. The excess of events for both experiments is close to their experimental energy threshold and can be attributed to a relatively light WIMP

with a mass of $\mathcal{O}(10)$ keV. Two further experiments have shown signal excesses above their expected background expectations: CRESST [79] and CDMS-Si [80]. Both consist of cryogenic bolometers operating at mK temperatures to measure the phonon signal of a possible dark matter particle-interaction. In addition to the phonon signal, scintillation light of the $CaWO_4$ crystals is also detected in the case of CRESST and a charge signal in the silicon crystals of CDMS-Si. Both techniques provide discrimination between signal and background events. Using a maximum likelihood analysis, a statistical significance of more than 4σ is found in the CRESST experiment. It has to be noted that the experiment had a rather high background, out of 67 accepted events ~ 44 were attributed to background. The reconstructed WIMP mass would be at rather low values (few to tens of GeV/c^2, see figure 3.3 right).

In contrast to the results listed above, there are a number of experiments where no evidence for dark matter was found although the same regions of cross section and WIMP mass were tested. Only a selection of results, including the ones with highest sensitivity, are mentioned here. Two-phase liquid xenon detectors as XENON10 [81], XENON100 [82] and LUX [83] have set over the last years most constraining upper limits on the cross section of WIMPs with matter. Although a low energy threshold analysis was performed by XENON10 [81], the main strength of liquid xenon detectors rely on their large detector masses and high atomic mass which gives excellent sensitivity to WIMP masses at $\sim 40\,\mathrm{GeV}/c^2$. The working principle of this technology, specifically of XENON100, is described in chapter 2. Detectors using germanium bolometers can reach very low energy thresholds and therefore have very good sensitivities down to few GeV/c^2 WIMPs. Early 2014, the SuperCDMS [84] collaboration has derived an upper limit from data in the energy region $(1.6 - 10)\,\mathrm{keV}_{nr}$ which strongly disfavours the signal indications at low WIMP masses. When interpreting the results as being due to spin dependent WIMP interactions, liquid xenon detectors are most sensitive for neutron coupling. For proton coupling, bubble chambers (COUPP [85], Picasso [86] and SIMPLE [87]) show the best results (see figure 3.4).

The results of, for example, LUX/XENON and DAMA and other signal indications are in strong tension when comparing the data in the spin-independent or spin-dependent scenarios. Another approach would be to explain the results as being due to a light dark matter particle like axions or axion-like particles. These particles would interact with electrons instead of nuclei, and the signal would be hidden in the region where γ-rays and electrons from natural radioactivity appear. In this context, discrimination between electronic and nuclear recoils is not required and the key signature is the annual modulation of the signal. Section 4.1 reviews searches of this type. It has to be noted as well that a different coupling of the dark matter particle to matter could eventually relax the tension between existing results. An example is the isospin-violating dark matter scenario in which the WIMP couples differently to protons and neutrons [88]. Other approaches assume that either the dark matter particles scatter to lower (inelastic dark matter [89]) or higher (exothermic dark matter [90]) excited states, or that the nuclei get excited to a higher state [91] (see also section 3.5).

Chapter 2

The XENON experiment

During the last years, the XENON100 direct dark matter detection experiment has set most stringent upper limits on the interaction cross section of dark matter with known matter. Recently, this result has been confirmed and improved by the LUX experiment which uses the same technology. This chapter starts summarising the advantages of using liquid xenon as detector medium. Next, the XENON100 working principle and the experimental setup are described. In the last section, important performance parameters such as stability, resolution and event position reconstruction are discussed.

2.1 Liquid xenon as detector material

Among the various detector materials in use, liquid xenon (LXe) combines a high WIMP sensitivity with an excellent self-shielding capability for background reduction. In the liquid state, xenon has a density of $2.8\,\mathrm{g/cm^3}$ and stops very efficiently external radiation, for example γ-rays. LXe can be used to build large (up to $\sim$ ton scale [92]) homogeneous detectors in a relatively easy way (e.g. compared to solid state detectors) as its temperature at $-100°\mathrm{C}$ can be reached using commercial cooling devices or liquid nitrogen. Its scintillation light is in the ultraviolet at a wavelength of 178 nm [93] and can therefore be detected directly with photomultipliers without the need of a wavelength-shifter.

Due to the A^2 enhancement of the cross section for spin-independent interactions, the large atomic mass of xenon offers a high sensitivity to this process. Furthermore, natural xenon contains almost 50% of non zero spin isotopes, ^{129}Xe and ^{131}Xe, providing sensitivity to spin-dependent WIMP interactions [94]. The only unstable isotope is the double-beta decaying ^{136}Xe which has, however, a lifetime of 2.1×10^{21} years [95]. This long lifetime results into a negligible count rate in the XENON100 detector. The only relevant internal radioactive contaminations are ^{85}Kr impurities in the xenon and radon emanated from construction materials.

2.2 The XENON100 instrument

The XENON100 detector consists of a two-phase liquid-xenon time projection chamber (TPC). If a charged particle deposits energy in the medium, both excitation and ionization of the xenon atoms occur. Xe^* excited atoms combine with neutral ones, Xe, producing excimers Xe_2^* which relaxate producing ultraviolet photons (S1). Similarly, ionised Xe^+ atoms form Xe_2^+ which recombines with nearby electrons producing additional scintillation photons [96]. In a TPC, a drift field is applied in order to transport the produced electrons from the interaction site to the detection plane. The electron charge cloud is extracted from the liquid to the gas phase using a stronger field. In the gas phase, the charge signal is amplified and converted to a secondary light pulse (S2) via proportional scintillation [97].

The simultaneous detection of prompt scintillation light and ionization signals provides discrimination between signal and background events as their relative size depends on the particle/interaction type (related to $\mathrm{d}E/\mathrm{d}x$). XENON100 uses a drift field of about 0.5 kV/cm and an extraction field in the gas gap of about 10 kV/cm [98]. Figure 2.1 shows a schematic view of the two-phase TPC working principle (left), a diagram of the difference

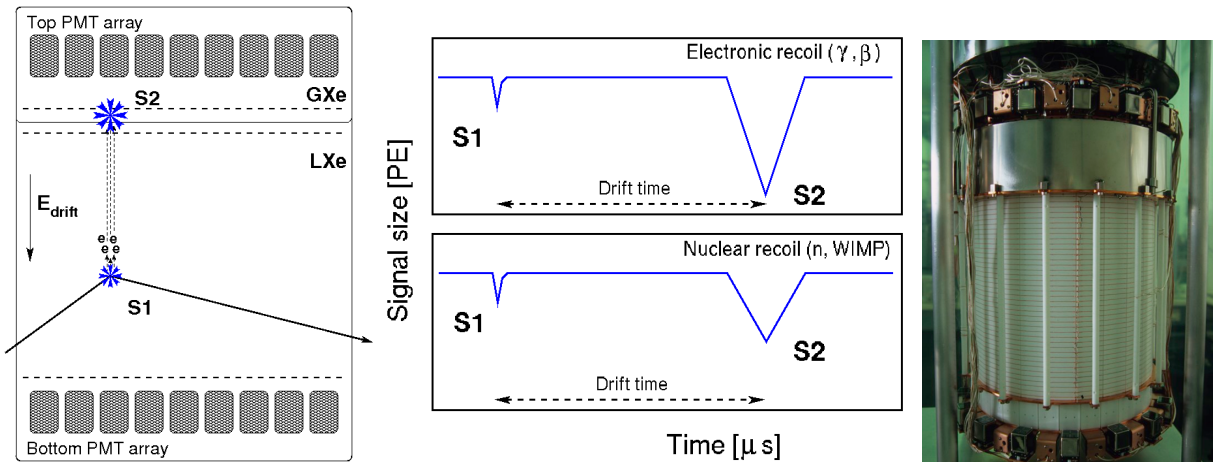

Figure 2.1: (Left) Working principle of a xenon two-phase liquid-gas TPC. (Middle) Schematic waveforms of scintillation (S1) and charge signal (S2) for electronic recoils and nuclear recoils. The ratio between both signal sizes allow to discriminate these two types of interactions. (Right) Photograph of the XENON100 TPC.

between an electronic and a nuclear recoil (middle) and a photograph of the XENON100 TPC structure (right). Both S1 and S2 are measured by two arrays of R8520 Hamamatsu photomultipliers (PMTs) placed on top and bottom of the TPC.

The detector is located at the underground 'Laboratori Nazionale del Gran Sasso' [1] in Italy to shield the experiment from cosmic radiation. The total mass of liquid xenon is 161 kg of which 62 kg are contained inside the TPC. The remaining 99 kg of the xenon provide an active veto of 4 cm thickness surrounding the TPC [99]. Teflon panels are used

[1] http://www.lngs.infn.it

in the TPC cage as UV-light reflector and to host field shaping rings which guarantee an uniform drift field. The xenon is liquified with a cooling system which uses a pulse tube refrigerator. The whole cryogenic vessel is placed inside a shield consisting of an inner copper layer, lead, polyethylene and an outer neutron-shield made out of water canisters. Before filling the detector, the xenon is purified to reduce its krypton contamination using a dedicated cryogenic distillation column. Thanks to careful screening and selection of radio-pure detector materials [100], the experiment achieved an electronic recoil background of $5.3 \times 10^{-3}\,\text{events} \cdot \text{kg}^{-1} \cdot \text{keV}^{-1} \cdot \text{d}^{-1}$ in the WIMP-search energy range inside a central volume corresponding to 34 kg fiducial xenon mass [82]. More details about the background in XENON100 are given in section 3.3.

2.3 Detector performance

XENON100 has been operating since 2009. Results for two major data sets of 100 and 225 live days have been released [101][82] in which no evidence for dark matter was found. During data taking the detector has shown stable thermodynamic conditions (pressure and temperature variations below 1%) as well as stable high voltage. The gain of the PMTs was set to 2×10^6 and its stability was monitored using weekly LED calibrations. The purity of the liquid xenon increased continuously due to the purification through a hot zirconium getter which removes electronegative impurities.

Weekly ^{137}Cs calibration data were used to study the LXe purity level but also the stability/evolution of light yield and charge yield. Figure 2.2 (left) shows the light (S1) and charge (S2) signals for a ^{137}Cs calibration run. S1 and S2 at the full absorption peak are anti correlated. This is due to the recombination fluctuations at the interaction point: the larger the recombination of initially ionized electrons, the larger the light

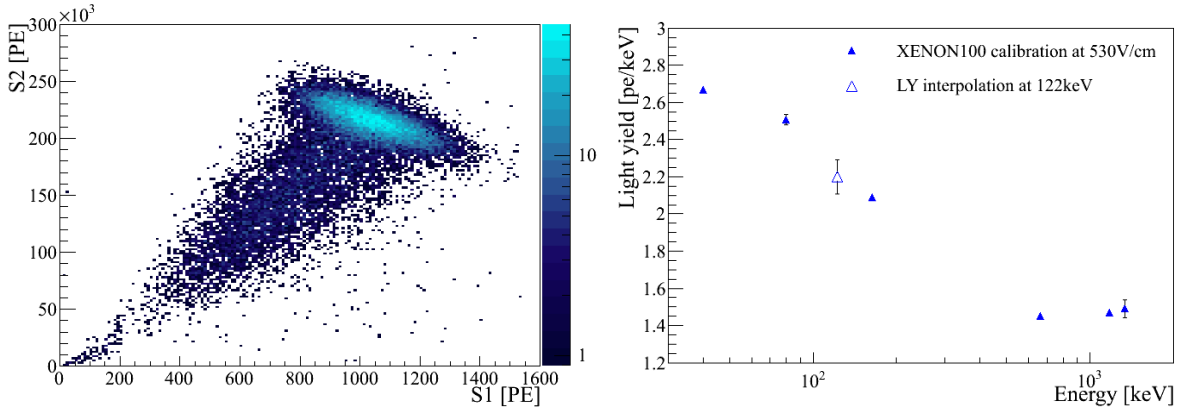

Figure 2.2: (Left) S2 versus S1 for the ^{137}Cs calibration source showing the anti-correlation between both signals for the full absorption peak at 662 keV energy. (Right) Light yield (S1) as function of energy for various mono-energetic lines as measured in XENON100 (filled marker) and the interpolation for 122 keV (empty marker).

signal and the smaller the extracted charge signal. The tail to low energies arises from Compton interactions where the scattered γ ray escapes the sensitive volume. The energy resolution at the full absorption peak of ^{137}Cs, 662 keV is 12.5% and 6.5% for S1 and S2, respectively. At 39.6 keV the resolutions decrease to about 15% for both signals [99]. The projection along the anti-correlation angle allows for an improved energy resolution of 2.3% at 662 keV. The light yield of the detector is evaluated at different energies using γ-ray sources (^{137}Cs and ^{60}Co) and inelastic scattering or de-excitation of metastable states created by neutrons from an AmBe calibration source. The later processes give mono energetic signals at 39.6 keV, 80.2 keV and 163.9 keV, see figure 2.2 (right). This electronic-recoil energy scale is relevant for dark matter searches where the expected signal arises from the energy deposition by electrons in the medium. However, as it is discussed in chapter 4, the energy region of interest is well below the measurements shown here.

For WIMP searches, a nuclear-recoil energy scale is needed. For practical reasons, this scale is anchored to the light yield of 122 keV γ-rays (see section 3.2). Due to the mean attenuation length of about 2.5 mm for these γ-rays in LXe, the detector cannot be calibrated with an external source. Therefore an interpolation of the light yield at this energy is necessary. This is performed using the calibration data showed in figure 2.2 and the 'noble element simulation technique', NEST, model for scintillation [102].

One of the advantages of TPCs is the possibility to precisely reconstruct the interaction vertex in order to select an innermost low-background volume for further analysis. In XENON100, the light pattern of the S2 signal in the top PMT array is used to determine the (x, y) position of the event with an uncertainty of 3 mm (see details of the methods in [99]). The z coordinate results from the time difference in the recorded position of the S1 and S2 signals and the known electron drift velocity. This coordinate is determined with an uncertainty of 0.3 mm. External background is reduced effectively by applying a fiducial volume cut based on the (x, y, z) reconstructed positions. As mentioned above, the outer region of the TPC is also instrumented with PMTs and it is used as active veto to reduce further the background from γ-interactions. Dedicated measurements using calibration γ-sources were performed to map the veto efficiency to tag γ interactions at different positions. A 70% background reduction in the energy region of interest for an inner fiducial volume < 50 kg is obtained [99].

Chapter 3

Searches for WIMPs in XENON100

This chapter describes the searches for WIMP candidates with the XENON100 detector. The data of two major science runs have been released so far, the first with 100 live days [101] in 2010 and the second during 2011 and 2012 with a total of 225 live days [82]. This chapter describes the data selection criteria for these runs, the nuclear recoil scale, the background prediction and the interpretation of the data are introduced. The results considering spin-independent and spin-dependent interactions are also presented as well as other tests and ongoing analyses.

3.1 Data selection and efficiency

The detector is calibrated with ^{137}Cs, ^{60}Co, ^{232}Th (gamma) and ^{241}AmBe (neutron) sources in order to characterize the detector performance, light and charge yields, their energy resolution, stability and position dependence. The attenuation of the charge signal due to residual impurities in the LXe and the nonuniform light collection of the S1 and S2 signals in the PMT arrays are corrected using maps from these calibration data. Furthermore, these data are used to determine the event selection criteria for dark matter searches and to define the signal and background regions in energy and discrimination parameters. The region of interest for signals from WIMP candidates was blinded to avoid biasing the analysis. The used science data were selected from periods of stable operating conditions considering detector thermodynamic properties, high voltage and background. The criteria to select candidate events include data quality including the removal of noise, energy range in S1 and S2, selection of single scatter events, consistency cuts and the selection of an inner fiducial volume for analysis [103]. The acceptance for all these cuts was calculated using mainly nuclear recoils from calibration data as they represent the WIMP recoil signature. The blue curve in figure 3.1 shows the summed cut acceptance of all criteria used in the second science run. The ionization threshold was lowered in this run by using a new hardware trigger condition such that the achieved efficiency was $> 99\%$ at 150 photoelectrons (PE) in S2. The efficiency curve of this S2 threshold cut is also shown in the figure (red curve). Note that this cut is independent

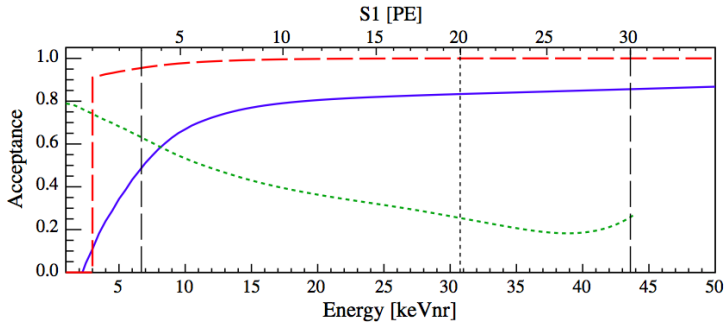

Figure 3.1: Energy dependence of the WIMP acceptance for all selection criteria (solid blue), for the S2 threshold condition (dashed red) and for a 99.75% rejection probability of electronic recoils (dotted green) during the 225 live days run. Figure from [82].

of possible fluctuations in the S1 signal and therefore has to be applied to the spectrum before taking S1 resolution into account.

3.2 Nuclear recoil energy scale

The nuclear recoil scale E_{nr} used for the analysis was calculated from the light signal (S1) using the equation $E_{nr} = (\mathrm{S1}/L_y)(1/L_{eff})(S_{ee}/S_{nr})$, where L_y is the light yield of a 122 keV γ ray at zero applied drift field. The term L_{eff} accounts for all quenching effects of the nuclear recoil scale. It is parametrized using all existing direct measurements from neutron scattering experiments at the time of publication (see [104] and references therein). S_{ee} and S_{nr} are the electric field scintillation quenching factors for electronic recoils and nuclear recoils, 0.58 and 0.95 [105], respectively, at the nominal field of 0.53 V/cm. In order to verify the energy scale used for the results mentioned above, a data/Monte Carlo comparison of the XENON100 nuclear recoil data acquired during the neutron source calibration with ^{241}AmBe has been performed [106]. The response of the XENON100 experiment was modelled using a detailed geometry of the whole experiment including the shield and the generation of the two signals S1 and S2. The calculated acceptance for the data was also applied to the Monte Carlo generated events.

In a first step, the S2 Monte Carlo spectrum is fitted to the corresponding data. From this procedure, the number of escaping electrons per unit energy, i.e. the charge yield Q_y, is extracted (see figure 3.2, left). Best spectral matching was obtained for a neutron source rate of 159 n/s. This number is in agreement with an independent measurement of the rate performed at the German National Metrology Institute, PTB, which yielded (160 ± 4) n/s. Using the derived Q_y, the S1 spectrum of the ^{241}AmBe nuclear recoils is similarly fitted to the Monte Carlo data and the scintillation efficiency L_{eff} is calculated. As it can be seen in figure 3.2 (right), the best-fit curve is in agreement with the energy scale used in previous XENON100 analyses [82] and with calculations using the correlation of ionization and scintillation [107] (dashed line in figure 3.2, left). In both steps comparing

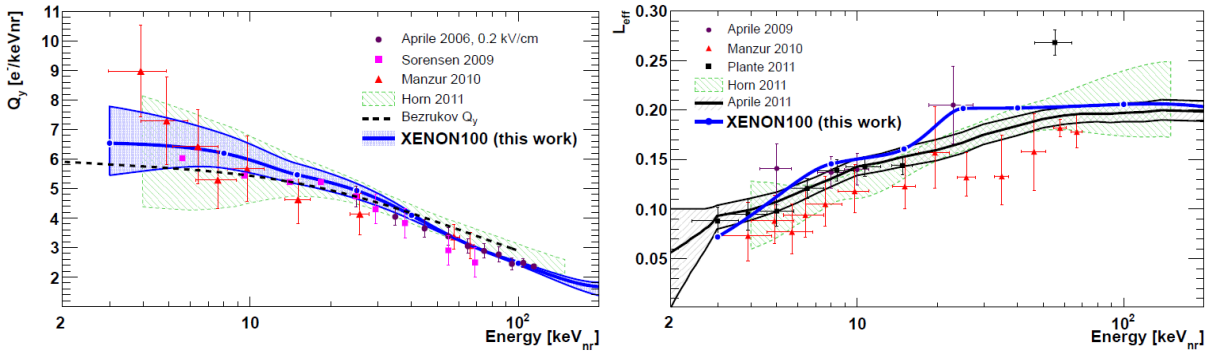

Figure 3.2: (Left) Q_y obtained from fitting nuclear recoil data from a neutron source to the Monte Carlo-generated S2 spectrum. (Right) L_{eff} obtained from the Monte Carlo/data matching of the S1 spectrum. Figures from [106].

Monte Carlo and data, a very good level of spectral shape matching is accomplished along with agreement in the 2-dimensional particle discrimination space. These results verified the calculated signal acceptance used by XENON100 for WIMP searches.

3.3 Background sources and experimental results

The total background to the dark matter signal region in the XENON100 experiment is calculated taking into account two types of sources: nuclear recoils from ambient or muon-induced neutrons and electronic recoils from γ and β decays in the LXe and surrounding materials. The nuclear recoil contribution is determined using Monte Carlo simulations and includes (α, n) reactions, spontaneous fission and fast neutrons from muon spallation reactions [108]. The electronic recoil background can be divided into external and internal sources. The external background, which is the dominant background of the experiment (about 55%), consists of Compton interactions from γ-rays emitted from radio-impurities in the detector construction materials. The contribution from the PMTs make up $\sim 65\%$ of this component [109]. Internal backgrounds are potentially more dangerous as they cannot be reduced by a fiducial volume cut. Radon is produced in the natural ^{238}U and ^{232}Th decay-chains and it is emanated from materials in contact with the LXe. This background contributes 30% in the low energy range of interest [110]. The beta decaying ^{85}Kr is mainly produced as a product of nuclear fission at power reactors and in nuclear weapons tests. A concentration of (14 ± 2) ppt $^{\text{nat}}$Kr in xenon [111] was achieved during the 225 live days run, which leads to a subdominant ^{85}Kr background ($\sim 15\%$). The electronic recoil background events are well described by a Gaussian function in the discrimination parameter variable (S2/S1). When this parameter is plotted versus S1 (energy) the so-called electronic recoil band is displayed (see black dots in figure 3.3 left). However, there are anomalous background events with an unusual low S2/S1 ratio. For example, incomplete charge collection below the cathode or at large radii results in low values of S2/S1 and leak into the region of interest. This anomalous events were modelled in the

discrimination versus S1 space using the observed event distribution in calibration data.

The primary analysis was decided 'a priori' to be based on a profile likelihood statistical treatment [112], however, a secondary analysis was also performed as a crosscheck using a benchmark WIMP search region. This region is confined by the dash lines in figure 3.3 (left) where the discrimination parameter as function of energy is shown. The benchmark WIMP search region was defined from $(6.6 - 30.5)\,\mathrm{keV}_{nr}$ in recoil energy and between an upper 99.75% electronic recoil rejection level (horizontal green line) and a lower 97% acceptance level derived from neutron calibration data (dashed blue line). The expected electronic and nuclear recoil background in the benchmark region are (0.79 ± 0.16) and $(0.17^{+0.12}_{-0.07})$ events, respectively, summing up to (1.0 ± 0.2) expected events. The profile likelihood method tested both the signal and the background-only hypothesis in the pre-defined energy range $(3 - 30)$ PE corresponding to $(6.6 - 43.3)\,\mathrm{keV}_{nr}$ recoil energy. Note that the upper energy bound is different from the one in the benchmark analysis as in the latter the bound was chosen to optimize the signal-to-background ratio. The background prediction included Gaussian and non-Gaussian components of the electronic recoil events leaking into the region of interest and nuclear recoils from neutrons reaching the innermost 34 kg fiducial mass used for the analysis. The event distribution after unblinding the dark matter data can be seen in figure 3.3. The profile likelihood analysis yielded a $p-$value of $\leq 5\%$ for all tested WIMP masses, indicating no signal over the predicted background. Two events fall in the benchmark WIMP-search region. The Poisson probability that the expected background of (1.0 ± 0.2) events fluctuates to 2 events is 26.4%, confirming the result of the profile likelihood analysis.

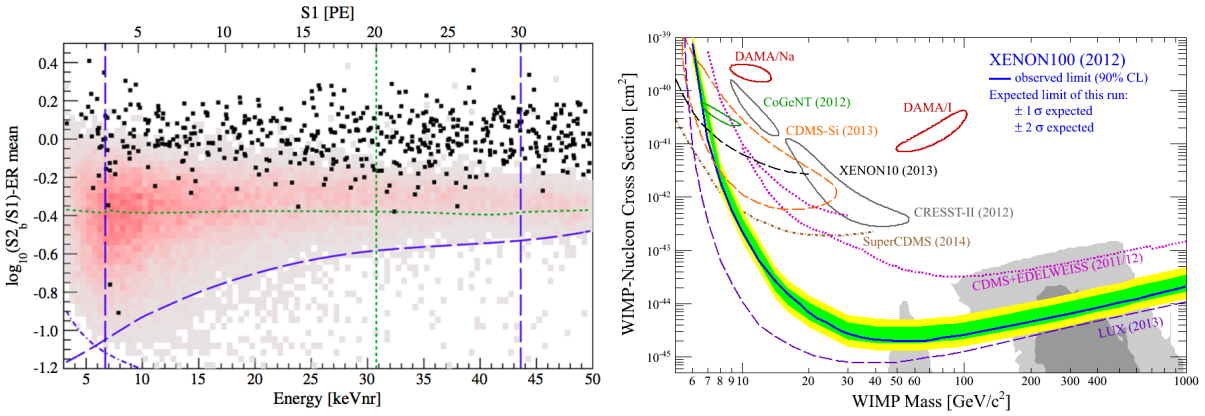

Figure 3.3: (Left) Event distribution in the discrimination parameter for the 225 live days data set using all selection criteria and a 34 kg fiducial volume. The meaning of the lines is described in the text. Figure from [82]. (Right) 90% C.L. exclusion limit for WIMP-nucleon spin independent cross section. The $1\sigma/2\sigma$ sensitivities are represented by the green/yellow bands. Figure adapted from [82] to include recent updates/results from XENON10 [81], CoGeNT [113], CDMS-Si [80], LUX [83] and SuperCDMS [84].

3.4 Spin independent and dependent interpretations

A 90% confidence level exclusion limit on the spin independent WIMP-nucleon cross section has been calculated assuming a standard isothermal WIMP halo with a local density of $0.3\,\mathrm{GeV/cm^3}$, a circular velocity of 220 km/s and an escape velocity of 544 km/s [65] (see also section 1.4). The limit includes systematic uncertainties in the energy scale L_{eff} and in the background expectation. The energy resolution, which is dominated by Poisson fluctuations in the number of PE, is taken into account. Figure 3.3 (right) shows the exclusion limit on spin-independent interaction process derived from the 225 live days dataset together with the $1\,\sigma$ and $2\,\sigma$ expected sensitivity in green and yellow, respectively. Results of other experiments including the recent XENON10 [81], CoGeNT [113], CDMS-Si [80], LUX [83] and SuperCDMS [84] exclusion limits and preferred regions by supersymmetric models (grey) are also depicted. The results from XENON100 and LUX are in tension with the signal indications from DAMA, CoGeNT, CDMS-Si and CRESST. Astrophysical uncertainties as mentioned in section 1.4 are not sufficient to resolve this tension [114].

Natural xenon contains two nonzero nuclear-spin isotopes, ^{129}Xe and ^{131}Xe, with an abundance of 26.4% and 21.2%, respectively. If WIMPs have spin, spin-dependent scattering with the isotopes mentioned above can occur. The results of the 225 live days run have been also interpreted on the model assumption of spin-dependent interactions [94]. The resulting exclusion limits, along with results from other experiments are shown in figure 3.4. Calculations of structure functions entering the spin-dependent cross section are

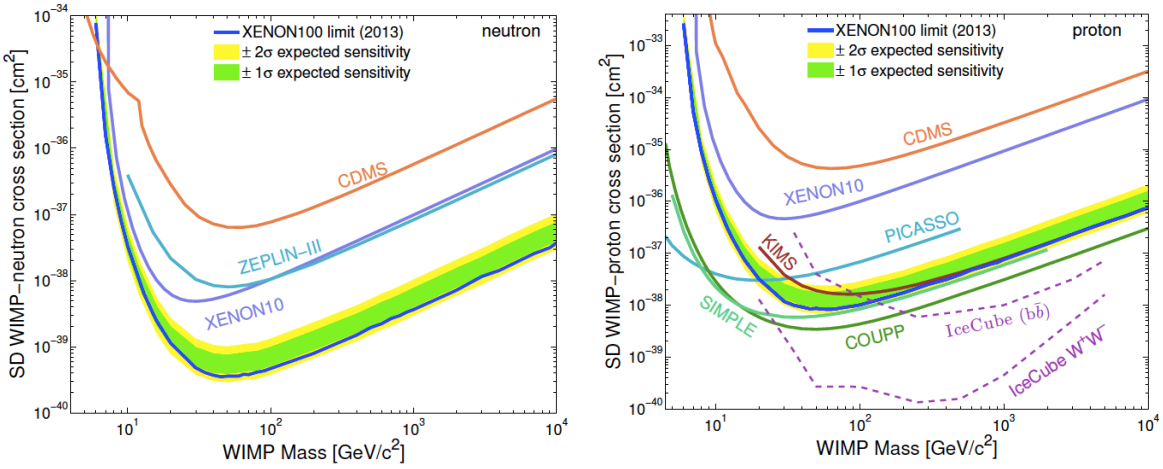

Figure 3.4: WIMP spin dependent 90% C.L. exclusion limits on cross section on neutrons (left) and protons (right). The green/yellow band represent the expected $1\sigma/2\sigma$ sensitivity for this run. Results of other direct detection experiments are included however different nuclear models are used, see [94]. The limits derived from the indirect search by the IceCube experiment [53] in the hard ($W^+W^-, \tau^+\tau^-$) and soft ($b\bar{b}$) annihilation channels are also displayed. Figures from [94].

commonly based on the nuclear shell model. For the limit derivation, recent results [115] using state-of-the-art valence shell interactions were employed. These new calculations yield a superior agreement between calculated and measured spectra for ^{129}Xe and ^{131}Xe both in energy and ordering of the nuclear levels [75]. If the DAMA signal is interpreted as being due to spin-dependent interactions, the cross section is around $2 \times 10^{-35}\,\mathrm{cm}^2$ and $10^{-36}\,\mathrm{cm}^2$ at $\sim 13\,\mathrm{GeV}/c^2$ WIMP mass for neutron and proton coupling, respectively [116]. Therefore also in this interpretation, the result of XENON100 disfavours the one of DAMA.

In order to increase the sensitivity and continue testing theoretically-favoured parameter regions of cross section and WIMP mass, the XENON collaboration is currently constructing the XENON1T detector. Chapter 5 describes the main characteristics of this future experiment.

3.5 Other interpretations of the XENON100 data

To overcome the experimental discrepancies mentioned in the previous section, an inelastic dark matter scattering was proposed [89]. This approach assumes that WIMPs can only scatter off nuclei by simultaneously getting excited to a higher state with an energy δ above the ground state. In this scenario, the elastic scattering would be highly suppressed or even forbidden. Contrary to the elastic case where the expected spectrum is exponential, the velocity threshold for the inelastic scattering process lead to an spectrum which is suppressed at low energies. The 100 live days dataset of XENON100 was used to place limits on inelastic dark matter [117]. This data ruled out at 90% C.L. the observed DAMA annual modulation signal as being due to inelastic dark matter particles.

Another direct detection possibility is the observation of inelastic WIMP-nucleus scattering inducing transitions to low-lying nuclear excited states [91]. The signature of such detection channel is a nuclear recoil followed by a γ-ray from the prompt de-excitation. In natural xenon, the ^{129}Xe and ^{131}Xe isotopes are ideal targets as they provide sufficiently low states at 39.6 keV and 80.2 keV, respectively. Recently the inelastic structure functions have been calculated for xenon [118]. Currently, the analysis using XENON100 data is on-going and results will be released soon.

An approach followed by the XENON10 experiment to gain sensitivity to low WIMP masses is the use of the amplified charge scale (S2) [81][119], see also black curve in figure 3.3. This method gives up the discrimination as the light signal for such small energies is below the experimental threshold. At lowest S2 energies, a new background producing single-electron signals appears. XENON100 has recently studied the origin and rate of these signals and the dominant contribution arises from photoionization of impurities in the LXe [98]. This is the first step in order to quantify the background towards the lowest S2 energies. On-going analysis will provide results on very low mass WIMPs in the near future.

Chapter 4

Light dark matter particles inducing electronic recoils

In the previous chapter, the elastic scattering of WIMP particles off nuclei has been considered, where the signal signature is a nuclear recoil. However, dark matter could consist of particles which interact predominantly with shell electrons in the detector target. In order to study the sensitivity of XENON100 to electronic interactions, the response of liquid xenon down to $\sim$keV electronic recoil energies needs to be measured. Two experiments pursuing this goal are presented, one using a low energy calibration source and one realized as a Compton coincidence setup. Finally, the energy threshold for XENON100 is calculated and its physical implications are discussed.

4.1 Motivation

As introduced in section 1.2, axion or axion-like particles are suitable dark matter candidates. They could have been produced non-thermally in the early Universe [42] with a small velocity dispersion and could therefore be warm or cold dark matter candidates. There are three types of searches for axions: laboratory-based experiments, for example [120], experiments detecting solar or galactic axions and finally constrains from astrophysical observations. For the latter, deviations in the properties of stars from theoretical predictions due to energy losses via the new particle are used [36]. Currently only null results have been produced but sensitivities are continuously improving. For a review of axion searches, see chapter 23 of [46]. Dark matter detectors belong to the second type of experiments mentioned above as they can look for signatures of axions interacting with the target via Compton-like, axioelectric (also photoelectric-like) or Primakov processes [121]. These processes involve only the emission of electrons and X-rays and can therefore not be separated from the experimental electronic recoil background. The interior of stars, like our Sun, is expected to be a powerful source of solar axions. This is due to the presence of strong electromagnetic fields which may convert the abundant photons into

axions. Searches for solar axions have been performed at different experiments [122] [123], however, the focus in this chapter is on the dark matter axion.

The annual modulation result of DAMA is strongly disfavoured by the XENON100 results when it is interpreted as being due to spin-independent or dependent interaction of WIMPs with target nuclei (see chapter 3). However, the DAMA experiment does not discriminate between nuclear recoils and electronic recoils as just the NaI scintillation signal is acquired. Therefore, a light dark matter candidate producing electronic recoils could be a possible explanation for the DAMA annual-modulated signal in the $(2-6)\,\mathrm{keV}$ energy region [77]. Axion-like particles, in particular with a mass of the order of keV/c^2 have been proposed as an explanation for the DAMA signal [121]. The favoured region in the axio-electric coupling, $g_{a\bar{e}e}$, versus axion mass parameter-space covers few orders of magnitude. Axion masses up to $7\,\mathrm{keV}/c^2$ are allowed with $g_{a\bar{e}e}$ around $\sim 10^{-10}$. For lower axion masses the coupling becomes larger, e.g. at $0.4\,\mathrm{keV}/c^2$ the coupling is around $\sim 10^{-8}$ [121]. Several detectors consisting of germanium crystals have performed similar searches and have placed upper limits on $g_{a\bar{e}e}$ disfavouring the DAMA result (CoGeNT [124], CDMS [123] and EDELWEISS [125]).

The axion hypothesis could be tested with liquid xenon detectors, for instance, by analysing the electronic recoil spectrum in the XENON100 data as the event rate at the lowest energies is lower than the one in DAMA [77]. However, first the energy threshold of XENON has to be measured to verify if both experiments test similar energy regions. Calibration sources used to characterise the XENON100 detector give mono energetic lines with the lowest energy at 39.6 keV being due to inelastic scattering of neutrons on ^{129}Xe (see section 2.3). To understand the behaviour of the energy scale below 39.6 keV, dedicated low-energy calibrations have to be performed.

4.2 Low energy calibration sources

In a first attempt to characterise the light yield and field quenching of liquid xenon (LXe) at low energies, the short-lived ^{83m}Kr source has been used [126]. This source has a transition at 32.1 keV followed by a 9.4 keV de-excitation after a half life of 154 ns. Being a noble gas like xenon, ^{83m}Kr disperses uniformly in all regions of the detector. A small scale (0.1 kg) LXe time projection chamber was setup at the University of Zurich to measure these transitions. The ^{83m}Kr was introduced in the chamber through the xenon purification system. Even for low source activities, the delayed signal coincidence provides a method of identifying these decays free of background. An example of a waveform with 10 ns sampling rate and the signal signature can be seen in figure 4.1 (left). Besides the determination of the energy scale, it is a challenging task to perform a detector calibration in the appropriate energy range for dark matter searches. Due to the inhomogeneous light collection, the detector response can vary significantly in various locations within the device. Therefore, a spatially uniform calibration that adequately probes all regions of the detector is important. ^{83m}Kr fulfils this requirement and is therefore an ideal

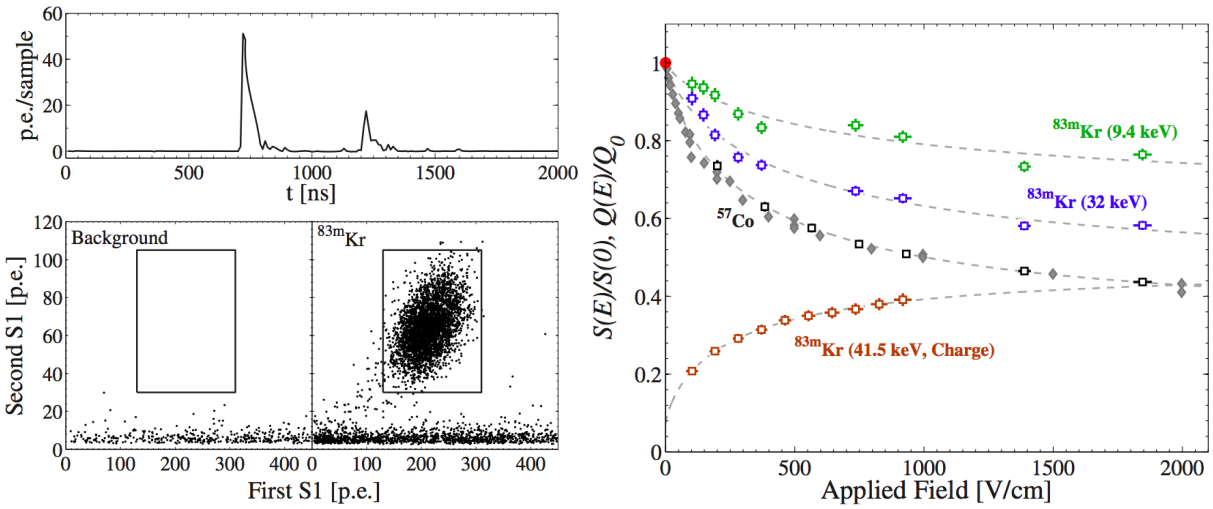

Figure 4.1: (Top left) Waveform of a typical ^{83m}Kr event. Below the event distribution of the data without and with source is shown. The clear delayed-coincidence signature gives a background-free measurement. (Right) Field quenching for ^{57}Co and the ^{83m}Kr transitions. Figures from [126].

calibration source to define spatial signal-corrections both in S1 and in S2.

The light yield of the two transitions of ^{83m}Kr has been studied for different drift fields. Figure 4.1 (right) shows the light field quenching for the 122 keV full absorption line of ^{57}Co and the 9.4 and 32.1 keV transitions of ^{83m}Kr. Due to the short lifetime of the 32.1 keV state of 154 ns and the width of the S2 signals ($\sim 1\,\mu$s), the charge signals for both interactions can not be disentangled. Therefore, the field quenching for the combined signal at 41.5 keV is given for the S2 signal. For decreasing energies, the LXe light yield increases, while the amount of electric field quenching is diminished. The data is modelled [126] using a three-parameter function based on the Thomas-Imel box model [127] for electron-ion recombinations. The dashed lines in figure 4.1 (right) are the fit results using this empirical model which does not contain LXe physical properties.

A further investigation of the light yield of the 9.4 keV line showed that its S1 signal-size depends on the time distance to the 32.1 keV de-excitation. This first de-excitation can leave a cloud of electron-ion pairs which haven't recombined by the time the second transition occur. This cloud would enhance the recombination of the 9.4 keV line resulting in a higher light yield [128]. Therefore, only the 32.1 keV line can be used as a low energy and uniformly distributed source for calibration but not the 9.4 keV transition. In the last years, ^{83m}Kr has been used to calibrate noble-gas dark matter detectors as the LUX [83] and the liquid argon experiment Dark Side-50. XENON100 is also planning to employ such a calibration in order to validate the corrections applied to the data.

4.3 Measurement of the electronic recoil scale using a Compton experiment

To understand the behaviour of the light yield below $\sim 30\,\text{keV}$, a Compton coincidence experiment has been performed at the University of Zurich. A 17.3 MBq gamma source (^{137}Cs) has been used where photons interact via Compton scattering in LXe and are then registered in a NaI coincidence detector [128]. For a well-known position the source and the coincidence detector, the scattering angle is known and the kinematics of the scattering in LXe are fixed. With this method, mono-energetic electronic recoils can be selected. Figure 4.2 shows a schematic view of the setup. The results of the experiment

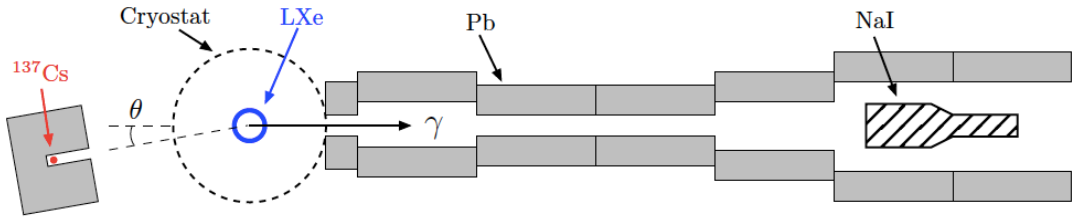

Figure 4.2: Top view of the experimental setup in the Compton coincidence experiment. Figure from [128].

show that at zero drift field, the light yield at 10 keV decreases to 40% of its value at higher energies. The left part of figure 4.3 shows the scintillation output, R_e, relative to that of 32 keV (red data points). These observations are compatible within $2\,\sigma$ with independent results using a similar technique [129] (violet diamonds). The light yield of the calibrations sources at 122 keV and 32.1 keV agree well with the results of Compton scattering. However, the light yield of 9.4 keV is clearly off due to the enhancement of the light yield as a consequence of a previous de-excitation as described in section 4.2. The green line shows the outcome of the latest version of the NEST empirical model [102].

As explained in section 2.2, liquid xenon TPCs use a drift field to gain the discrimination capability between electronic and nuclear recoils. Using an applied electric field of 450 V/cm [128] which is close to the field of 530 V/cm used in XENON100, the scintillation output is reduced to about 75% relative to the value at zero field. Figure 4.3 shows the reduction of the scintillation output relative to the one at zero drift field, q, due to field quenching at 450 V/cm. Despite of the light yield reduction, liquid xenon shows a non negligible scintillation at few keV energies in a presence of the tested drift field.

4.4 Energy threshold of XENON100

Using the energy scale shown in figure 4.3, the electronic recoil threshold of XENON100 has been calculated [128]. XENON100 uses a slightly different electric field than the results shown above, 530 V/cm instead of 450 V/cm. Therefore, an extrapolation of the

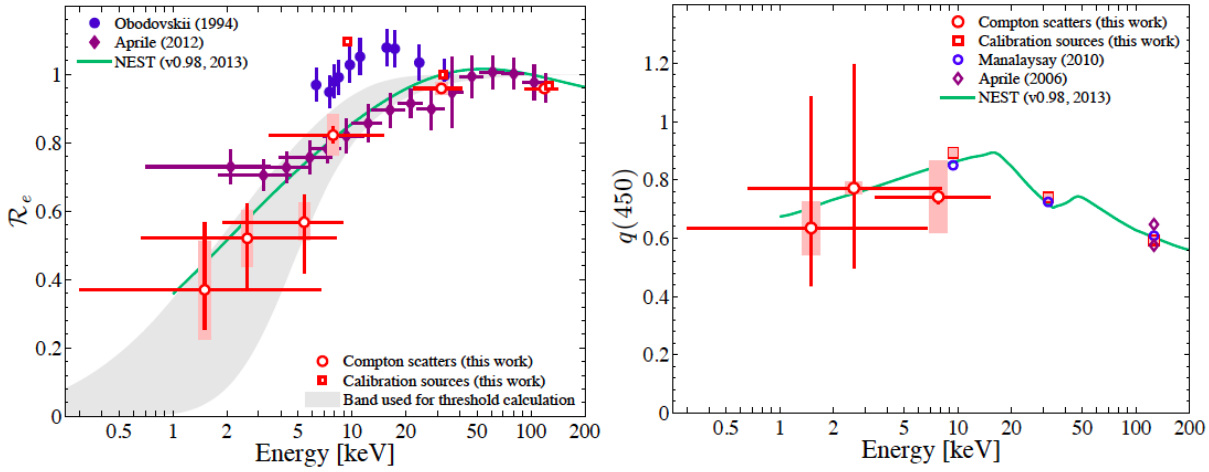

Figure 4.3: (Left) Energy dependence of the scintillation yield for electronic recoils at zero drift-field. The results are relative to the light yield of 32 keV. (Right) Field quenching at 450 V/cm as function of energy. Figures from [128]. In both figures the statistical uncertainties are represented by red vertical lines, the systematic uncertainties are the shaded rectangles, and the $1\,\sigma$ spread in energy as horizontal lines.

field quenching is required. Although this correction is small it has been applied using an empirical parametrisation of the field quenching. An energy threshold of $2.3^{+0.4}_{-0.3}$ keV is derived for XENON100 [126]. The error on this value results from the uncertainty band shown in grey in figure 4.3. This S1 energy threshold and the recoil scale derived above can be used to test the axion hypothesis in XENON100. Especially the axion interpretation of the DAMA signal at $(2-6)$ keV can be probed. Several analyses of this type, i.e. searches for solar axions and rate modulation studies, are currently on-going. First results are expected within 2014.

An energy scale determined in a laboratory experiment can introduce uncertainties due to the different light yield and drift field values compared to the dark matter detector. Therefore, it would be ideal to have an in-situ calibration of the energy scale in XENON100. This can be performed using double scattered events from a ^{137}Cs source [130]. The light pulses (S1s) of the two vertices can not be separated due to the scintillation time constant of the LXe of several ns. However, the charge pulses (S2s) can be distinguished if their interaction heights, z coordinate, differs more than 3 mm from each other. For a known source position and a precise reconstruction of the two vertices in the LXe, the kinematics of the first Compton-interaction can be fully reconstructed. By selecting different scattering angles, the charge yield at various energy events can be measured. For higher energies above 40 keV, the mono-energetic calibration sources mentioned in section 2.3 can be used as a cross check. The resolution of the S2 energy scale at low energies is similar to the S1 but a scale determined directly at XENON100 would involve, in principle, less uncertainties than one determined externally.

Chapter 5

Summary and outlook

A clear evidence for the existence of dark matter from Astronomy and Cosmology observations has triggered large experimental and theoretical efforts to understand its nature. If dark matter is a particle, liquid xenon is an excellent medium for its detection. XENON100 is a two-phase xenon TPC, aiming for a direct detection of dark matter via its scattering off target particles. The results on WIMP searches assuming both spin-independent and spin-dependent interactions are presented in this work. Until the recent results of the LUX experiment [83], XENON100 has been leading WIMP-nucleon cross section sensitivity of dark matter scattering off nuclei reaching an upper limit for spin-independent cross section of $2 \times 10^{-45}\,\mathrm{cm}^2$ at $55\,\mathrm{GeV}/c^2$ WIMP mass [82]. The nuclear recoil scale used for the analysis is derived using data from laboratory neutron-scattering experiments [104]. This scale has been recently validated by fitting Monte Carlo data to the XENON100 spectrum of an ^{241}AmBe neutron source [106]. The good agreement with the previously used scale verifies the robustness of the WIMP search analysis. Nevertheless, dark matter could consist of particles which interact with electrons instead of nuclei (as WIMPs). To search for this type of particles, the electronic recoil scale in liquid xenon is required. Light-yield results for electronic recoils down to 1.5 keV have been used to determine the energy threshold of XENON100 which is around 2.3 keV [128]. The analysis of XENON100 data using this scale is ongoing.

Currently, XENON100 continues operation and is taking dark matter data. In order to increase the sensitivity significantly, the XENON collaboration has started to build a next generation detector, XENON1T [92], consisting of about 3 tons of LXe. The design consists of a dual-phase TPC of about 1 m height and about 1 m in diameter with a fiducial mass of about 1 ton. The goal is to reduce the background by a factor of ~ 100 compared to XENON100 where an ultra-low background at the level of 5×10^{-3} events/(keV·kg·d) [82] has been measured. This is possibly achieved by using an additional water muon-veto detector, improved material screening and selection, and by reducing the intrinsic contamination with ^{85}Kr and radon using dedicated removal devices (e.g. via cryogenic distillation [131]). In XENON100, the radioactivity from construction materials, specifically of the photosensors, contributes largely to the background spectrum. Therefore, a new 3-inch high quantum efficiency and low radioactive PMT has been developed in col-

laboration with the Hamamatsu company to further reduce the background. This R11410 tube have been extensively measured to confirm its reliable operation in LXe [132]. With XENON1T, the goal is to probe spin-independent WIMP-nucleon cross sections down to $2 \times 10^{-47}\,\mathrm{cm}^2$ for a $50\,\mathrm{GeV/c}^2$ WIMP mass. Figure 5.1 shows the projected sensitivity by using a 2.2 ton-year exposure, 99.75% background rejection rejection in log(S2/S1) discrimination parameter and 40% efficiency to detect nuclear recoils. The construction

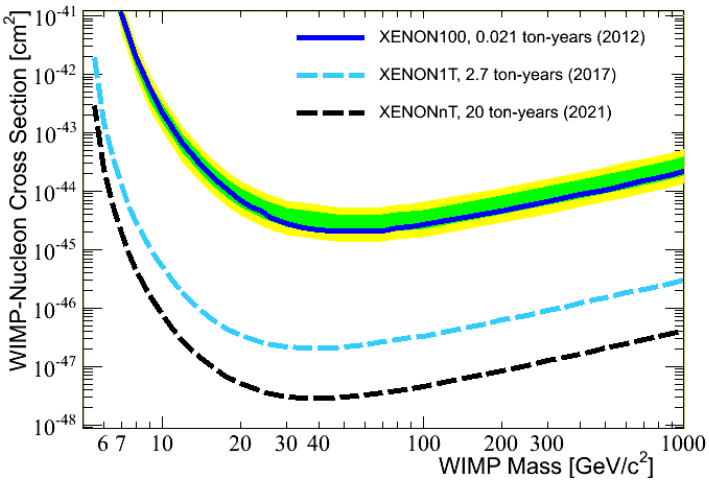

Figure 5.1: Projected sensitivity for spin independent WIMP-nucleon cross section with the XENON1T and the XENONnT experiments. Figure adapted from [133].

of the infrastructure for XENON1T has started in summer 2013 at the Laboratori Nationale del Gran Sasso in Italy and by the time of writing (March 2014), the water tank is completed and the infrastructure building is under construction. The start of data taking is planned for 2015. An upgrade to XENONnT having approx. 6 tons fiducial volume is already planned and the XENON1T setup is designed to easily accommodate this larger detector (sensitivity shown also in figure 5.1).

The success of the liquid noble gas TPC technology has motivated further proposals for even larger detectors like MAX [134] in the US and DARWIN [135] in Europe consisting of large liquid xenon and argon detectors. In the case of dark matter signal evidence in XENON1T, the DARWIN (dark matter WIMP search with noble liquids) experiment which foresees a total mass of about 20 tons, could make a high statistics measurement of its particle properties, i.e. its mass and cross section. In addition, the capability of the liquid xenon part of DARWIN for other physics channels including neutrinos have been studied [136]. The solar pp-neutrino flux could be measured for instance with a statistical uncertainty of around 1% after 5 years of data, reaching the precision of solar model predictions. Solar neutrinos will, however, constitute a limiting background to dark matter searches for cross sections below $\sim 2\times10^{-48}\,\mathrm{cm}^2$ and WIMP masses around 50 GeV. Coherent scattering of neutrinos on xenon will also limit the sensitivity to WIMP masses below ~ 6 GeV to cross sections above $\sim 4\times10^{-45}\,\mathrm{cm}^2$. In addition, a half-life sensitivity of 5.6×10^{26} y to the neutrinoless double beta decay of ^{136}Xe after 5 years of data could be reached using an innermost 6 tons mass in order to reduce external backgrounds.

Bibliography

[1] J. Oort, "The force exerted by the stellar system in the direction perpendicular to the galactic plane and some related problems," *Bull. of the Astron. Inst. of the Netherlands* **6** (1932) 249.

[2] F. Zwicky, "Die Rotverschiebung von extragalaktischen Nebeln," *Helvetica Physica Acta* **6** (1933) 110.

[3] V. C. Rubin, N. Thonnard, and J. Ford, W. K., "Extended rotation curves of high-luminosity spiral galaxies.," *Astrophys. J* **225** (1978) L107.

[4] M. Bartelmann and P. Schneider, "Weak gravitational lensing," *Phys. Rept.* **340** (2001) 291, arXiv:astro-ph/9912508.

[5] A. Einstein, "Lens-Like Action of a Star by the Deviation of Light in the Gravitational Field," *Science* **84** (1936) 506.

[6] F. Zwicky, "Nebulae as gravitational lenses," *Phys. Rev.* **51** (1937) 290.

[7] D. Clowe, M. Bradac, A. H. Gonzalez, M. Markevitch, S. W. Randall, *et al.*, "A direct empirical proof of the existence of dark matter," *Astrophys. J.* **648** (2006) L109, arXiv:astro-ph/0608407.

[8] M. Bradac, S. W. Allen, T. Treu, H. Ebeling, R. Massey, *et al.*, "Revealing the properties of dark matter in the merging cluster MACSJ0025.4-1222," *Astrophys. J.* **687** (2008) 959, arXiv:0806.2320.

[9] W. A. Dawson, D. Wittman, M. Jee, P. Gee, J. P. Hughes, *et al.*, "Discovery of a Dissociative Galaxy Cluster Merger with Large Physical Separation," *Astrophys. J.* **747** (2012) L42, arXiv:1110.4391.

[10] A. Mahdavi, H. Hoekstra, A. Babul, D. Balam, and P. Capak, "A Dark Core in Abell 520," *Astrophys. J.* **668** (2007) 806, arXiv:0706.3048.

[11] C.-J. Ma, H. Ebeling, and E. Barrett, "An X-ray/optical study of the complex dynamics of the core of the massive intermediate-redshift cluster MACSJ0717.5+3745," *Astrophys. J.* **693** (2009) L56, arXiv:0901.4783.

[12] M. Jee, A. Mahdavi, H. Hoekstra, A. Babul, J. Dalcanton, *et al.*, "A Study of the Dark Core in A520 with Hubble Space Telescope: The Mystery Deepens," *Astrophys. J.* **747** (2012) 96, arXiv:1202.6368.

[13] D. Clowe, M. Markevitch, M. Bradac, A. H. González, S. M. Chung, *et al.*, "On Dark Peaks and Missing Mass: A Weak Lensing Mass Reconstruction of the Merging Cluster System Abell 520," *Astrophys. J.* **758** (2012) 128, arXiv:1209.2143.

[14] **WMAP** Collaboration, G. Hinshaw *et al.*, "Nine-Year Wilkinson Microwave Anisotropy Probe (WMAP) Observations: Cosmological Parameter Results," *Astrophys. J. Suppl.* **208** (2013) 19, arXiv:1212.5226.

[15] **Planck** Collaboration, P. Ade *et al.*, "Planck 2013 results. I. Overview of products and scientific results," arXiv:1303.5062.

[16] **Supernova Search** Collaboration, A. G. Riess *et al.*, "Observational evidence from supernovae for an accelerating universe and a cosmological constant," *Astron. J.* **116** (1998) 1009, arXiv:astro-ph/9805201.

[17] **Planck** Collaboration, P. Ade *et al.*, "Planck 2013 results. XV. CMB power spectra and likelihood," arXiv:1303.5075.

[18] V. Springel, C. S. Frenk, and S. D. White, "The large-scale structure of the Universe," *Nature* **440** (2006) 1137, arXiv:astro-ph/0604561.

[19] V. Springel, S. D. White, A. Jenkins, C. S. Frenk, N. Yoshida, *et al.*, "Simulating the joint evolution of quasars, galaxies and their large-scale distribution," *Nature* **435** (2005) 629, arXiv:astro-ph/0504097.

[20] **2dFGRS** Collaboration, M. Colless, B. A. Peterson, C. Jackson, J. A. Peacock, S. Cole, *et al.*, "The 2dF Galaxy Redshift Survey: Final data release," arXiv:astro-ph/0306581.

[21] R.-y. Cen, J. Miralda-Escude, J. P. Ostriker, and M. Rauch, "Gravitational collapse of small scale structure as the origin of the Lyman alpha forest," *Astrophys. J.* **437** (1994) L9, arXiv:astro-ph/9409017.

[22] L. Van Waerbeke, Y. Mellier, and H. Hoekstra, "Dealing with systematics in cosmic shear studies: New results from the VIRMOS-Descart survey," *Astron. Astrophys.* **429** (2005) 75, arXiv:astro-ph/0406468.

[23] A. Pontzen and F. Governato, "Cold dark matter heats up," *Nature* **506** (2014) 171, arXiv:1402.1764.

[24] B. Paczynski, "Gravitational microlensing by the galactic halo," *Astrophys. J.* **304** (1986) 1.

[25] **MACHO** Collaboration, C. Alcock *et al.*, "The MACHO project: Microlensing results from 5.7 years of LMC observations," *Astrophys. J.* **542** (2000) 281, arXiv:astro-ph/0001272.

[26] M. Milgrom, "A Modification of the Newtonian dynamics as a possible alternative to the hidden mass hypothesis," *Astrophys. J.* **270** (1983) 365.

[27] J. D. Bekenstein, "Relativistic gravitation theory for the MOND paradigm," *Phys. Rev.* **D70** (2004) 083509, arXiv:astro-ph/0403694.

[28] S. D. White, C. Frenk, and M. Davis, "Clustering in a Neutrino Dominated Universe," *Astrophys. J.* **274** (1983) L1.

[29] S. Tremaine and J. E. Gunn, "Dynamical role of light neutral leptons in cosmology," *Phys. Rev. Lett.* **42** (1979) 407.

[30] A. Kusenko, "Sterile neutrinos: The Dark side of the light fermions," *Phys. Rept.* **481** (2009) 1, arXiv:0906.2968.

[31] K. Abazajian, G. M. Fuller, and W. H. Tucker, "Direct detection of warm dark matter in the X-ray," *Astrophys. J.* **562** (2001) 593, arXiv:astro-ph/0106002.

[32] G. Gelmini and P. Gondolo, "DM Production Mechanisms," arXiv:1009.3690.

[33] G. Jungman, M. Kamionkowski, and K. Griest, "Supersymmetric dark matter," *Phys. Rept.* **267** (1996) 195, arXiv:hep-ph/9506380.

[34] C. Baker, D. Doyle, P. Geltenbort, K. Green, M. van der Grinten, *et al.*, "An Improved experimental limit on the electric dipole moment of the neutron," *Phys. Rev. Lett.* **97** (2006) 131801, arXiv:hep-ex/0602020.

[35] R. Peccei and H. R. Quinn, "CP Conservation in the Presence of Instantons," *Phys. Rev. Lett.* **38** (1977) 1440.

[36] G. G. Raffelt, "Astrophysical axion bounds," *Lect. Notes Phys.* **741** (2008) 51, arXiv:hep-ph/0611350.

[37] S. Weinberg, "A New Light Boson?," *Phys. Rev. Lett.* **40** (1978) 223.

[38] J. E. Kim, "Weak Interaction Singlet and Strong CP Invariance," *Phys. Rev. Lett.* **43** (1979) 103.

[39] M. A. Shifman, A. Vainshtein, and V. I. Zakharov, "Can Confinement Ensure Natural CP Invariance of Strong Interactions?," *Nucl. Phys.* **B166** (1980) 493.

[40] A. Zhitnitsky, "On Possible Suppression of the Axion Hadron Interactions. (In Russian)," *Sov. J. Nucl. Phys.* **31** (1980) 260.

[41] M. Dine, W. Fischler, and M. Srednicki, "A Simple Solution to the Strong CP Problem with a Harmless Axion," *Phys. Lett.* **B104** (1981) 199.

[42] P. Sikivie, "Experimental Tests of the Invisible Axion," *Phys. Rev. Lett.* **51** (1983) 1415.

[43] L. Abbott and P. Sikivie, "A Cosmological Bound on the Invisible Axion," *Phys. Lett.* **B120** (1983) 133.

[44] L. Visinelli and P. Gondolo, "Dark Matter Axions Revisited," *Phys. Rev.* **D80** (2009) 035024, arXiv:0903.4377.

[45] S. Arrenberg, L. Baudis, K. Kong, K. T. Matchev, and J. Yoo, "Kaluza-Klein Dark Matter: Direct Detection vis-a-vis LHC (2013 update)," arXiv:1307.6581.

[46] G. Bertone, ed., *Particle dark matter*. Cambridge University Press, 2010.

[47] **CMS** Collaboration, S. Chatrchyan *et al.*, "The CMS experiment at the CERN LHC," *JINST* **3** (2008) S08004.

[48] **ATLAS** Collaboration, G. Aad *et al.*, "The ATLAS Experiment at the CERN Large Hadron Collider," *JINST* **3** (2008) S08003.

[49] **CMS** Collaboration, S. Chatrchyan *et al.*, "Observation of a new boson at a mass of 125 GeV with the CMS experiment at the LHC," *Phys. Lett.* **B716** (2012) 30, arXiv:1207.7235.

[50] **ATLAS** Collaboration, G. Aad *et al.*, "Observation of a new particle in the search for the Standard Model Higgs boson with the ATLAS detector at the LHC," *Phys. Lett.* **B716** (2012) 1, arXiv:1207.7214.

[51] **CMS** Collaboration, S. Chatrchyan *et al.*, "Search for dark matter and large extra dimensions in monojet events in pp collisions at $\sqrt{s} = 7$ TeV," *JHEP* **1209** (2012) 094, arXiv:1206.5663.

[52] **ATLAS** Collaboration, G. Aad *et al.*, "Search for dark matter candidates and large extra dimensions in events with a photon and missing transverse momentum in pp collision data at $\sqrt{s} = 7$ TeV with the ATLAS detector," *Phys. Rev. Lett.* **110** (2013) 011802, arXiv:1209.4625.

[53] **IceCube** Collaboration, M. Aartsen *et al.*, "Search for dark matter annihilations in the Sun with the 79-string IceCube detector," *Phys. Rev. Lett.* **110** (2013) 131302, arXiv:1212.4097.

[54] **MAGIC** Collaboration, J. Aleksic *et al.*, "Searches for Dark Matter annihilation signatures in the Segue 1 satellite galaxy with the MAGIC-I telescope," *JCAP* **1106** (2011) 035, arXiv:1103.0477.

[55] **H.E.S.S.** Collaboration, A. Abramowski *et al.*, "Search for photon line-like signatures from Dark Matter annihilations with H.E.S.S," *Phys. Rev. Lett.* **110** (2013) 041301, arXiv:1301.1173.

[56] **Veritas** Collaboration, T. Arlen *et al.*, "Constraints on Cosmic Rays, Magnetic Fields, and Dark Matter from Gamma-Ray Observations of the Coma Cluster of Galaxies with VERITAS and Fermi," *Astrophys. J.* **757** (2012) 123, arXiv:1208.0676.

[57] **Fermi-LAT** Collaboration, M. Ackermann *et al.*, "Dark Matter Constraints from Observations of 25 Milky Way Satellite Galaxies with the Fermi Large Area Telescope," *Phys. Rev.* **D89** (2014) 042001, arXiv:1310.0828.

[58] **Fermi-LAT** Collaboration, "Search for Gamma-ray Spectral Lines with the Fermi Large Area Telescope and Dark Matter Implications," *Phys. Rev.* **D88** (2013) 082002, arXiv:1305.5597.

[59] **PAMELA** Collaboration, O. Adriani *et al.*, "An anomalous positron abundance in cosmic rays with energies 1.5-100 GeV," *Nature* **458** (2009) 607, arXiv:0810.4995.

[60] **AMS** Collaboration, M. Aguilar *et al.*, "First Result from the Alpha Magnetic Spectrometer on the International Space Station: Precision Measurement of the Positron Fraction in Primary Cosmic Rays of 0.5350 GeV," *Phys. Rev. Lett.* **110** (2013) 141102.

[61] M. W. Goodman and E. Witten, "Detectability of Certain Dark Matter Candidates," *Phys. Rev.* **D31** (1985) 3059.

[62] A. Drukier, K. Freese, and D. Spergel, "Detecting Cold Dark Matter Candidates," *Phys. Rev.* **D33** (1986) 3495.

[63] D. N. Spergel, "The Motion of the Earth and the Detection of Wimps," *Phys. Rev.* **D37** (1988) 1353.

[64] J. Lewin and P. Smith, "Review of mathematics, numerical factors, and corrections for dark matter experiments based on elastic nuclear recoil," *Astropart. Phys.* **6** (1996) 87.

[65] A. M. Green, "Astrophysical uncertainties on direct detection experiments," *Mod. Phys. Lett.* **A27** (2012) 1230004, arXiv:1112.0524.

[66] F. J. Kerr and D. Lynden-Bell, "Review of galactic constants," *Mon. Not. Roy. Astron. Soc.* **221** (1986) 1023.

[67] M. C. Smith, G. Ruchti, A. Helmi, R. Wyse, J. Fulbright, *et al.*, "The RAVE Survey: Constraining the Local Galactic Escape Speed," *Mon. Not. Roy. Astron. Soc.* **379** (2007) 755, arXiv:astro-ph/0611671.

[68] V. Springel, J. Wang, M. Vogelsberger, A. Ludlow, A. Jenkins, *et al.*, "The Aquarius Project: the subhalos of galactic halos," *Mon. Not. Roy. Astron. Soc.* **391** (2008) 1685, arXiv:0809.0898.

[69] J. Stadel, D. Potter, B. Moore, J. Diemand, P. Madau, *et al.*, "Quantifying the heart of darkness with GHALO - a multi-billion particle simulation of our galactic halo," *Mon. Not. Roy. Astron. Soc.* **398** (2009) L21, arXiv:0808.2981.

[70] J. Diemand, M. Kuhlen, P. Madau, M. Zemp, B. Moore, *et al.*, "Clumps and streams in the local dark matter distribution," *Nature* **454** (2008) 735, arXiv:0805.1244.

[71] J. F. Navarro, C. S. Frenk, and S. D. White, "The Structure of cold dark matter halos," *Astrophys. J.* **462** (1996) 563, arXiv:astro-ph/9508025.

[72] R. H. Helm, "Inelastic and Elastic Scattering of 187-MeV Electrons from Selected Even-Even Nuclei," *Phys. Rev.* **104** (1956) 1466.

[73] M. Ressell and D. Dean, "Spin dependent neutralino - nucleus scattering for A approximately 127 nuclei," *Phys. Rev.* **C56** (1997) 535, arXiv:hep-ph/9702290.

[74] P. Toivanen, M. Kortelainen, J. Suhonen, and J. Toivanen, "Large-scale shell-model calculations of elastic and inelastic scattering rates of lightest supersymmetric particles (LSP) on I-127, Xe-129, Xe-131, and Cs-133 nuclei," *Phys. Rev.* **C79** (2009) 044302.

[75] J. Menéndez, D. Gazit, and A. Schwenk, "Spin-dependent WIMP scattering off nuclei," *Phys. Rev.* **D86** (2012) 103511, arXiv:1208.1094.

[76] P. J. Fox, J. Liu, and N. Weiner, "Integrating Out Astrophysical Uncertainties," *Phys. Rev.* **D83** (2011) 103514, arXiv:1011.1915.

[77] **DAMA/LIBRA** Collaboration, R. Bernabei *et al.*, "New results from DAMA/LIBRA," *Eur. Phys. J.* **C67** (2010) 39, arXiv:1002.1028.

[78] **CoGeNT** Collaboration, C. Aalseth *et al.*, "Search for An Annual Modulation in Three Years of CoGeNT Dark Matter Detector Data," arXiv:1401.3295.

[79] **CRESST** Collaboration, G. Angloher, M. Bauer, I. Bavykina, A. Bento, C. Bucci, *et al.*, "Results from 730 kg days of the CRESST-II Dark Matter Search," *Eur. Phys. J.* **C72** (2012) 1971, arXiv:1109.0702.

[80] **CDMS** Collaboration, R. Agnese *et al.*, "Silicon Detector Dark Matter Results from the Final Exposure of CDMS II," *Phys. Rev. Lett.* **111** (2013) 251301, arXiv:1304.4279.

[81] **XENON10** Collaboration, J. Angle *et al.*, "A search for light dark matter in XENON10 data," *Phys. Rev. Lett.* **107** (2011) 051301, arXiv:1104.3088.

[82] **XENON100** Collaboration, E. Aprile *et al.*, "Dark Matter Results from 225 Live Days of XENON100 Data," *Phys. Rev. Lett.* **109** (2012) 181301, arXiv:1207.5988.

[83] **LUX** Collaboration, D. Akerib *et al.*, "First results from the LUX dark matter experiment at the Sanford Underground Research Facility," arXiv:1310.8214.

[84] **SuperCDMS** Collaboration, R. Agnese *et al.*, "Search for Low-Mass WIMPs with SuperCDMS," arXiv:1402.7137.

[85] **COUPP** Collaboration, E. Behnke *et al.*, "First Dark Matter Search Results from a 4-kg CF_3I Bubble Chamber Operated in a Deep Underground Site," *Phys. Rev.* **D86** (2012) 052001, arXiv:1204.3094.

[86] **PICASSO** Collaboration, S. Archambault *et al.*, "Constraints on Low-Mass WIMP Interactions on ^{19}F from PICASSO," *Phys. Lett.* **B711** (2012) 153, arXiv:1202.1240.

[87] **SIMPLE** Collaboration, M. Felizardo, T. Girard, T. Morlat, A. Fernandes, A. Ramos, *et al.*, "Final Analysis and Results of the Phase II SIMPLE Dark Matter Search," *Phys. Rev. Lett.* **108** (2012) 201302, arXiv:1106.3014.

[88] J. L. Feng, J. Kumar, D. Marfatia, and D. Sanford, "Isospin-Violating Dark Matter," *Phys. Lett.* **B703** (2011) 124, arXiv:1102.4331.

[89] D. Tucker-Smith and N. Weiner, "Inelastic dark matter," *Phys. Rev.* **D64** (2001) 043502, arXiv:hep-ph/0101138.

[90] P. W. Graham, R. Harnik, S. Rajendran, and P. Saraswat, "Exothermic Dark Matter," *Phys. Rev.* **D82** (2010) 063512, arXiv:1004.0937.

[91] J. R. Ellis, R. Flores, and J. Lewin, "Rates for Inelastic Nuclear Excitation by Dark Matter Particles," *Phys. Lett.* **B212** (1988) 375.

[92] **XENON1T** Collaboration, E. Aprile *et al.*, "The XENON1T Dark Matter Search Experiment," arXiv:1206.6288.

[93] O. Cheshnovsky, B. Raz, and J. Jortner, "Temperature dependence of rare gas molecular emission in the vacuum ultraviolet," *Chem. Phys. Lett.* **15** (1972) 475.

[94] **XENON100** Collaboration, E. Aprile *et al.*, "Limits on spin-dependent WIMP-nucleon cross sections from 225 live days of XENON100 data," *Phys. Rev. Lett.* **111** (2013) 021301, arXiv:1301.6620.

[95] **EXO** Collaboration, M. Auger *et al.*, "Search for Neutrinoless Double-Beta Decay in ^{136}Xe with EXO-200," *Phys. Rev. Lett.* **109** (2012) 032505, arXiv:1205.5608.

[96] S. Kubota, A. Nakamoto, T. Takahashi, T. Hamada, E. Shibamura, M. Miyajima, K. Masuda, and T. Doke, "Recombination luminescence in liquid argon and in liquid xenon," *Phys. Rev.* **B17** (1978) 2762.

[97] A. Lansiart, A. Seigneur, J.-L. Moretti, and J.-P. Morucci, "Development research on a highly luminous condensed xenon scintillator," *Nucl. Instrum. Meth.* **135** (1976) 47.

[98] **XENON100** Collaboration, E. Aprile *et al.*, "Observation and applications of single-electron charge signals in the XENON100 experiment," *J. Phys. G: Nucl. Part. Phys.* **41** (2014) 035201, arXiv:1311.1088.

[99] **XENON100** Collaboration, E. Aprile *et al.*, "The XENON100 Dark Matter Experiment," *Astropart. Phys.* **35** (2012) 573, arXiv:1107.2155.

[100] **XENON100** Collaboration, E. Aprile *et al.*, "Material screening and selection for XENON100," *Astropart. Phys.* **35** (2011) 43, arXiv:1103.5831.

[101] **XENON100** Collaboration, E. Aprile *et al.*, "Dark Matter Results from 100 Live Days of XENON100 Data," *Phys. Rev. Lett.* **107** (2011) 131302, arXiv:1104.2549.

[102] M. Szydagis, A. Fyhrie, D. Thorngren, and M. Tripathi, "Enhancement of nest capabilities for simulating low-energy recoils in liquid xenon," *JINST* **8** (2013) C10003, arXiv:1307.6601.

[103] **XENON100** Collaboration, E. Aprile *et al.*, "Analysis of the XENON100 Dark Matter Search Data," *Astropart. Phys.* **54** (2014) 11, arXiv:1207.3458.

[104] G. Plante, E. Aprile, R. Budnik, B. Choi, K. Giboni, *et al.*, "New Measurement of the Scintillation Efficiency of Low-Energy Nuclear Recoils in Liquid Xenon," *Phys. Rev.* **C84** (2011) 045805, arXiv:1104.2587.

[105] E. Aprile, C. Dahl, L. DeViveiros, R. Gaitskell, K. Giboni, *et al.*, "Simultaneous measurement of ionization and scintillation from nuclear recoils in liquid xenon as target for a dark matter experiment," *Phys. Rev. Lett.* **97** (2006) 081302, arXiv:astro-ph/0601552.

[106] **XENON100** Collaboration, E. Aprile *et al.*, "Response of the XENON100 Dark Matter Detector to Nuclear Recoils," *Phys. Rev.* **D88** (2013) 012006, arXiv:1304.1427.

[107] F. Bezrukov, F. Kahlhoefer, and M. Lindner, "Interplay between scintillation and ionization in liquid xenon Dark Matter searches," *Astropart. Phys.* **35** (2011) 119, arXiv:1011.3990.

[108] **XENON100** Collaboration, E. Aprile *et al.*, "The neutron background of the XENON100 dark matter search experiment," *J. Phys.* **G40** (2013) 115201, arXiv:1306.2303.

[109] **XENON100** Collaboration, E. Aprile *et al.*, "Study of the electromagnetic background in the XENON100 experiment," *Phys. Rev.* **D83** (2011) 082001, arXiv:1101.3866.

[110] M. Weber, *Gentle neutron signals and noble background in the XENON100 dark matter experiment*. PhD thesis, University of Heidelberg, 2013.

[111] S. Lindemann and H. Simgen, "Krypton assay in xenon at the ppq level using a gas chromatographic system combined with a mass spectrometer," *Eur. Phys. J. C* **74** no. 2, (2014) 1, arXiv:1308.4806.

[112] **XENON100** Collaboration, E. Aprile *et al.*, "Likelihood Approach to the First Dark Matter Results from XENON100," *Phys. Rev.* **D84** (2011) 052003, arXiv:1103.0303.

[113] **CoGeNT** Collaboration, C. Aalseth *et al.*, "CoGeNT: A Search for Low-Mass Dark Matter using p-type Point Contact Germanium Detectors," *Phys. Rev.* **D88** (2013) 012002, arXiv:1208.5737.

[114] M. T. Frandsen, F. Kahlhoefer, C. McCabe, S. Sarkar, and K. Schmidt-Hoberg, "The unbearable lightness of being: CDMS versus XENON," *JCAP* **1307** (2013) 023, arXiv:1304.6066.

[115] P. Klos, J. Menéndez, D. Gazit, and A. Schwenk, "Large-scale nuclear structure calculations for spin-dependent WIMP scattering with chiral effective field theory currents," *Phys. Rev.* **D88** (2013) 083516, arXiv:1304.7684.

[116] M. R. Buckley and W. H. Lippincott, "A Spin-Dependent Interpretation for Possible Signals of Light Dark Matter," *Phys. Rev.* **D88** (2013) 056003, 1306.2349.

[117] **XENON100** Collaboration, E. Aprile *et al.*, "Implications on Inelastic Dark Matter from 100 Live Days of XENON100 Data," *Phys. Rev.* **D84** (2011) 061101, arXiv:1104.3121.

[118] L. Baudis, G. Kessler, P. Klos, R. Lang, J. Menéndez, *et al.*, "Signatures of Dark Matter Scattering Inelastically Off Nuclei," arXiv:1309.0825.

[119] R. Essig, A. Manalaysay, J. Mardon, P. Sorensen, and T. Volansky, "First Direct Detection Limits on sub-GeV Dark Matter from XENON10," *Phys. Rev. Lett.* **109** (2012) 021301, arXiv:1206.2644.

[120] **ADMX** Collaboration, S. Asztalos *et al.*, "A SQUID-based microwave cavity search for dark-matter axions," *Phys. Rev. Lett.* **104** (2010) 041301, arXiv:0910.5914.

[121] R. Bernabei, P. Belli, F. Montecchia, F. Nozzoli, F. Cappella, *et al.*, "Investigating pseudoscalar and scalar dark matter," *Int. J. Mod. Phys.* **A21** (2006) 1445, arXiv:astro-ph/0511262.

[122] K. Abe, K. Hieda, K. Hiraide, S. Hirano, Y. Kishimoto, *et al.*, "Search for solar axions in XMASS, a large liquid-xenon detector," *Phys. Lett. B* **724** (2013) 46, arXiv:1212.6153.

[123] **CDMS** Collaboration, Z. Ahmed *et al.*, "Search for Axions with the CDMS Experiment," *Phys. Rev. Lett.* **103** (2009) 141802, arXiv:0902.4693.

[124] **CoGeNT** Collaboration, C. Aalseth *et al.*, "Experimental constraints on a dark matter origin for the DAMA annual modulation effect," *Phys. Rev. Lett.* **101** (2008) 251301, arXiv:0807.0879.

[125] **EDELWEISS-II** Collaboration, E. Armengaud *et al.*, "Axion searches with the EDELWEISS-II experiment," *JCAP* **1311** (2013) 067, arXiv:1307.1488.

[126] A. Manalaysay, T. Marrodán Undagoitia, A. Askin, L. Baudis, A. Behrens, *et al.*, "Spatially uniform calibration of a liquid xenon detector at low energies using ^{83m}Kr," *Rev. Sci. Instrum.* **81** (2010) 073303, arXiv:0908.0616.

[127] J. Thomas and D. Imel, "Recombination of electron-ion pairs in liquid argon and liquid xenon," *Phys. Rev.* **A36** (1987) 614.

[128] L. Baudis, H. Dujmovic, C. Geis, A. James, A. Kish, *et al.*, "Response of liquid xenon to Compton electrons down to 1.5 keV," *Phys. Rev.* **D87** (2013) 115015, arXiv:1303.6891.

[129] E. Aprile, R. Budnik, B. Choi, H. Contreras, K. Giboni, *et al.*, "Measurement of the Scintillation Yield of Low-Energy Electrons in Liquid Xenon," *Phys. Rev.* **D86** (2012) 112004, arXiv:1209.3658.

[130] L. Rauch Master's thesis, University of Heidelberg, 2014. to be submitted.

[131] **XMASS** Collaboration, K. Abe *et al.*, "Distillation of Liquid Xenon to Remove Krypton," *Astropart. Phys.* **31** (2009) 290, arXiv:0809.4413.

[132] L. Baudis, A. Behrens, A. Ferella, A. Kish, T. Marrodán Undagoitia, *et al.*, "Performance of the Hamamatsu R11410 Photomultiplier Tube in cryogenic Xenon Environments," *JINST* **8** (2013) P04026, arXiv:1303.0226.

[133] A. Brown, "private communication," 2013. Data from the XENON Collaboration.

[134] R. Alarcon *et al.*, "MAX: Multi-Ton Argon and Xenon," *FERMILAB-PROPOSAL-1001* (2009) .

[135] **Darwin** Collaboration, L. Baudis, "DARWIN: dark matter WIMP search with noble liquids," arXiv:1012.4764.

[136] L. Baudis, A. Ferella, A. Kish, A. Manalaysay, T. Marrodán Undagoitia, *et al.*, "Neutrino physics with multi-ton scale liquid xenon detectors," *JCAP* **01** (2014) 044, arXiv:1309.7024.

Appendices

Appendix A

Own contributions

The scientific results of XENON100 arise from a common effort of the collaboration which I joined in January 2009. My main contributions to the data analysis addressed different aspects related to the detector calibration and stability, the data selection and the study of different background populations. I used data from neutron and gamma calibration sources to determine different signal characteristics as, for example, light and charge yields, resolutions or spatial variations due to collection effects. Furthermore, I performed detailed studies of the detector stability concerning thermodynamic parameters, signal sizes, electronic noise, photomultiplier performance and high voltage. Using these studies I performed the data selection for the dark matter analysis. In addition, some of the event quality cuts were developed by me. I also contributed to the study of events with an anomalous charge to light ratio. My contributions to the data analysis are reflected in the XENON100 publications, in particular in the analysis paper for which I am a corresponding author.

Regarding the operation of XENON100, I participated in the regular shifts and the maintenance of the detector. Moreover, I was in charge of the calibration measurements in 2011. Currently, I coordinate the photosensor working group for the future XENON1T experiment, and I am responsible for the test of all 250 photomultiplier tubes needed for the detector.

For the two experiments performed at the University of Zurich, the ^{83m}Kr measurements and the Compton experiment, I contributed in several aspects. The system was partially built when I started to work in the group, thus I participated first in the hardware installations and the testing of the liquid xenon chamber. Then I took responsibility for the regular operations and the monitoring of the system which was running over many months. I also took part in the data analysis by performing independent cross checks. Finally, I contributed to the publications of the results.

Appendix B

Main publications summarised in this work

- *Dark Matter Results from 225 Live Days of XENON100 Data* [82],
  E. Aprile *et al.* (XENON100 Collaboration), Phys. Rev. Lett, **109** (2012) 181301, arXiv:1207.5988.

- *Limits on spin-dependent WIMP-nucleon cross sections from 225 live days of XENON100 data* [94],
  E. Aprile *et al.* (XENON100 Collaboration), Phys. Rev. Lett, **111** (2013) 021301, arXiv:1301.6620.

- *The XENON100 Dark Matter Experiment* [99],
  E. Aprile *et al.* (XENON100 Collaboration), Astropart. Phys. **35** (2012) 573, arXiv:1107.2155

- *Analysis of the XENON100 Dark Matter Search Data* [103],
  E. Aprile *et al.* (XENON100 Collaboration), Astropart. Phys. **54** (2014) 11, arXiv:1207.3458 *T. Marrodán Undagoitia corresponding author

- *Spatially uniform calibration of a liquid xenon detector at low energies using* ^{83m}Kr [126],
  A. Manalaysay, T. Marrodán Undagoitia, A. Askin, L. Baudis, A. Behrens, A.D. Ferella, A. Kish, O. Lebeda, R. Santorelli and D. Venos, Rev. Sci. Instrum. **81** (2010) 073303, arXiv:0908.0616

- *Response of liquid xenon to Compton electrons down to 1.5 keV* [128],
  L. Baudis, H. Dujmovic, C. Geis, A. James, A. Kish, A. Manalaysay, T. Marrodán Undagoitia and M. Schumann, Phys. Rev. **D87** (2013) 115015, arXiv:1303.6891.

Appendix C

Complete list of publications

- *Search for the proton decay $p \to K^+\overline{\nu}$ in the large liquid scintillator low energy neutrino astronomy detector LENA*, T. Marrodán Undagoitia *et al.*, Phys. Rev. **D72** (2005) 075014 arXiv:hep-ph/0511230.

- *Low energy neutrino astronomy with the large liquid-scintillation detector LENA*, T. Marrodán Undagoitia *et al.*, Prog. Part. Nucl. Phys. **57** (2006) 287, arXiv:hep-ph/0605229

- *Simulation of the proton decay in the LENA detector*, T. Marrodán Undagoitia *et al.*, Prog. Part. Nucl. Phys. **57** (2006) 290

- *Proton decay in the large liquid scintillator detector LENA: study of the background*, T. Marrodán Undagoitia *et al.*, Jour. of Phys. Conf. Ser. **39** (2006) 269

- *Low energy neutrino astronomy with the large liquid-scintillation detector LENA*, T. Marrodán Undagoitia *et al.*, Jour. of Phys. Conf. Ser. **39** (2006) 287

- *Probing the Earth's interior with the LENA detector*, K. A. Hochmuth *et al.*, Earth Moon Planets **99** (2006) 253, arXiv:hep-ph/0610048

- *Detection potential for the diffuse supernova neutrino background in the large liquid-scintillator detector LENA* , M. Wurm *et al.*, Phys. Rev. **D75** (2007) 023007, arXiv:astro-ph/0701305.

- *Probing the Earth's interior with a large-volume liquid scintillator detector*, K. Hochmuth *et al.*, Astropart. Phys. **27** (2007) 21 arXiv:hep-ph/0509136.

- *Large underground, liquid based detectors for astro-particle physics in Europe: Scientific case and prospects*, D. Autiero *et al.*, JCAP **0711** (2007) 011, arXiv:0705.0116.

- *LENA: A multipurpose detector for low energy neutrino astronomy and proton decay*, T. Marrodán Undagoitia *et al.*, Jour. of Phys. Conf. Ser. **120** (2008) 052018

- *Low energy Neutrino Astronomy in the future large-volume Liquid Scintillator Detector LENA*, M. Wurm *et al.*, Jour. of Phys. Conf. Ser. **136** (2008) 042071
- *Fluorescence decay-time constants in organic liquid scintillators*, T. Marrodán Undagoitia *et al.*, Rev. Sci. Instrum. **80** (2009) 043301, arXiv:0904.4602.
- *The LAGUNA design study – towards giant liquid based underground fetectors for neutrino physics and astrophysics and proton decay searches* (The LAGUNA consortium), D. Angus *et al.*, arXiv:1001.0077
- *Spectroscopy of electron-induced fluorescence in organic liquid scintillators*, T. Marrodán Undagoitia *et al.*, Eur. Phys. J. D **57** (2010) 105, arXiv:1001.3946.
- *Spatially uniform calibration of a liquid xenon detector at low energies using* ^{83m}Kr, A. Manalaysay *et al.*, Rev. Sci. Instrum. **81** (2010) 073303, arXiv: 0908.0616.
- *Optical Scattering Lengths in Large Liquid-Scintillator Neutrino Detectors*, M. Wurm *et al.*, Rev. Sci. Instrum. **81** (2010) 053301, arXiv:1004.0811.
- *First Dark Matter Results from the XENON100 Experiment*, E. Aprile *et al.* (XENON100 Collaboration), Phys. Rev. Lett. **105** (2010) 131302, arXiv:1005.0380.
- *Direct dark matter search using liquid noble gases*, T. Marrodán Undagoitia, PoS TEXAS **2010** (2010) 209.
- *Physics with the large liquid-scintillation detector LENA*, T. Lachenmeier *et al.*, Prog. Part. Nucl. Phys. **64** (2010) 381
- *Background Measurements in the Gran Sasso Underground Laboratory*, M. Haffke *et al.*, Nucl. Instrum. Meth. A **643** (2011) 36, arXiv:1101.5298.
- *Likelihood Approach to the First Dark Matter Results from XENON100*, E. Aprile *et al.* (XENON100 Collaboration), Phys. Rev. D **84** (2011) 052003, arXiv:1103.0303.
- *Gator: a low-background counting facility at the Gran Sasso Underground Laboratory*, L. Baudis *et al.*, JINST **6** (2011) P08010, arXiv:1103.2125.
- *Material screening and selection for XENON100*, E. Aprile *et al.* (XENON100 Collaboration), Astropart. Phys. **35** (2011) 43, arXiv:1103.5831.
- *Dark Matter Results from 100 Live Days of XENON100 Data*, E. Aprile *et al.* (XENON100 Collaboration), Phys. Rev. Lett. **107** (2011) 131302, arXiv:1104.2549.
- *Implications on Inelastic Dark Matter from 100 Live Days of XENON100 Data*, E. Aprile *et al.* (XENON100 Collaboration), Phys. Rev. D **84** (2011) 061101, arXiv:1104.3121.
- *Mini-review direct dark matter detection and recent XENON100 results*, T. Marrodán Undagoitia, PoS EPS-HEP **2011** (2011) 056.

- *LENA: Low Energy Neutrino Astronomy*, L. Oberauer *et al.*, Nucl. Phys. Proc. Suppl. **217** (2011) 127.
- *Direct dark matter search using liquid noble gases*, T. Marrodán Undagoitia, PoS TEXAS **2010** (2010) 209.
- *The XENON100 Dark Matter Experiment*, E. Aprile *et al.* (XENON100 Collaboration), Astropart. Phys. **35** (2012) 573, arXiv:1107.2155.
- *The next-generation liquid-scintillator neutrino observatory LENA*, M. Wurm *et al.*, Astropart. Phys. **35** (2012) 685, arXiv:1104.5620
- *Study of the electromagnetic background in the XENON100 experiment*, E. Aprile *et al.* (XENON100 Collaboration), Phys. Rev. D **83** (2011) 082001, [Erratum-ibid. D **85** (2012) 029904], arXiv:1101.3866.
- *Dark Matter Results from 225 Live Days of XENON100 Data*, E. Aprile *et al.* (XENON100 Collaboration), Phys. Rev. Lett, **109** (2012) 181301, arXiv:1207.5988.
- *The distributed Slow Control System of the XENON100 Experiment*, E. Aprile *et al.* (XENON100 Collaboration), JINST **7** (2012) T12001, arXiv:1211.0836.
- *Future neutrino physics with LENA (Low Energy Neutrino Astronomy)*, J. Winter *et al.*, Jour. of Phys. Conf. Ser. **375** (2012) 042052
- *Limits on spin-dependent WIMP-nucleon cross sections from 225 live days of XENON100 data*, E. Aprile *et al.* (XENON100 Collaboration), Phys. Rev. Lett, **111** (2013) 021301, arXiv:1301.6620.
- *Response of liquid xenon to Compton electrons down to 1.5 keV*, L. Baudis *et al.*, Phys. Rev. **D87** (2013) 115015, arXiv:1303.6891.
- *Performance of the Hamamatsu R11410 Photomultiplier Tube in cryogenic Xenon Environments*, L. Baudis *et al.*, JINST **8** 04026 (2013), arXiv:1303.0226.
- *Response of the XENON100 Dark Matter Detector to Nuclear Recoils*, E. Aprile *et al.* (XENON100 Collaboration), Phys. Rev. D **88** (2013) 012006, arXiv:1304.1427.
- *The neutron background of the XENON100 dark matter search experiment*, E. Aprile *et al.* (XENON100 Collaboration), J. Phys. G **40** (2013) 115201, arXiv:1306.2303.
- *Analysis of the XENON100 Dark Matter Search Data*, E. Aprile *et al.* (XENON100 Collaboration), Astropart. Phys. **54** (2014) 11, arXiv:1207.3458
- *Neutrino physics with multi-ton scale liquid xenon detectors*, L. Baudis *et al.* JCAP **01** (2014) 044, arXiv:1309.7024.
- *Observation and applications of single-electron charge signals in the XENON100 experiment*, E. Aprile *et al.* (XENON100 Collaboration), J. Phys. G **41** (2014) 035201, arXiv:1311.1088.

Acknowledgments

First of all I would like to thank Laura Baudis and Manfred Lindner for giving me the opportunity to work in their groups. I have profited a lot from very interesting discussions, suggestions and a motivating working environment.

From my colleagues at the University of Zurich, I want to specially thank Aaron Manalaysay and Marc Schumann. It was very nice to work with them, both doing measurements in the laboratory and discussing results in our office.

From my colleagues at MPIK Heidelberg, I want to thank Marc Weber, Ludwig Rauch, Wolfgang Hampel, Joachim Kopp and Quirin Weitzel for many interesting physics discussions and for their helpful comments on this work.

Finally, I want to thank my colleagues from the XENON collaboration for the nice teamwork. In a common effort, including many meetings and telephone conferences, we have produced great results with the XENON100 detector.